DISSERTATIONS IN
FORESTRY AND
NATURAL SCIENCES

JANNE LAUKKANEN

Fabrication of metallic micro- and nanostructures for optical solutions

PUBLICATIONS OF THE UNIVERSITY OF EASTERN FINLAND
Dissertations in Forestry and Natural Sciences

UNIVERSITY OF
EASTERN FINLAND

JANNE LAUKKANEN

Fabrication of metallic micro- and nanostructures for optical solutions

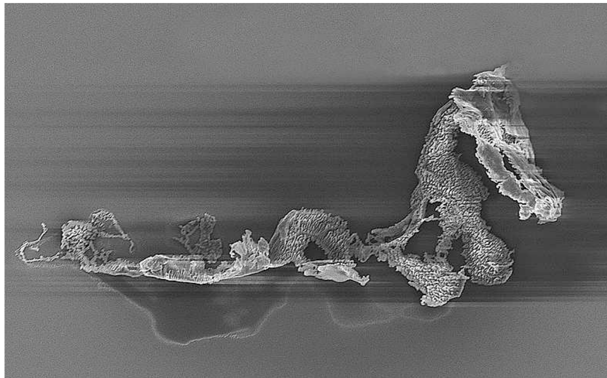

Publications of the University of Eastern Finland
Dissertations in Forestry and Natural Sciences
No 12

Academic Dissertation
To be presented by permission of the Faculty of Science and Forestry for public examination in the Auditorium M100 in Metria Building at the University of Eastern Finland, Joensuu, on October, 1, 2010,
at 12 o'clock noon.

Department of Physics and Mathematics

Kopijyvä Oy
Joensuu, 2010
Editors: Prof. Pertti Pasanen
Prof. Tarja Lehto, Prof. Kai Peiponen

Distribution:
University of Eastern Finland Library / Sales of publications
P.O. Box 107, FI-80101 Joensuu, Finland
tel. +358-50-3058396
http://www.uef.fi/kirjasto

ISBN: 978-952-61-0177-4 (printed)
ISSN: 1798-5668
ISBN: 978-952-61-0178-1 (pdf)
ISSN: 1798-5676
ISSNL: 1798-5668

Author's address: University of Eastern Finland
Department of Physics and Mathematics
P.O.Box 111
80101 JOENSUU
FINLAND
email: janne.laukkanen@uef.fi

Supervisors: Professor Jari Turunen, Dr. Tech.
University of Eastern Finland
Department of Physics and Mathematics
P.O.Box 111
80101 JOENSUU
FINLAND
email: jari.turunen@uef.fi

Professor Markku Kuittinen, Ph.D.
University of Eastern Finland
Department of Physics and Mathematics
P.O.Box 111
80101 JOENSUU
FINLAND
email: markku.kuittinen@uef.fi

Reviewers: Professor Jens Gobrecht, Dr.-Ing.
Paul Scherrer Institut
Laboratory for Micro- and Nanotechnology
5232 VILLIGEN PSI
SWITZERLAND
email: jens.gobrecht@psi.ch

Docent Ari Tervonen, Dr. Tech.
Aalto University
School of Science and Technology
Department of Micro and Nanosciences
Micronova
P.O.Box 13500
00076 AALTO
FINLAND
email: ari.tervonen@tkk.fi

Opponent: Professor Paul Urbach, Ph.D.
Delft University of Technology
Applied Sciences
Imaging Science and Technology
Lorentzweg 1
2628 CJ DELFT
THE NETHERLANDS
email: h.p.urbach@tudelft.nl

ABSTRACT

This work is focused on the fabrication of metallic micro- and nanostructures. Brief theoretical background is given for the presented applications. Patterning of the structures was done by electron beam lithography. Several fabrication methods of metal structures, including lift-off and dry etching, are discussed. Metallic structures are considered as final elements used in optical measurements and as mask or mould structures for post processing. Lift-off is the simplest method of fabrication for shallow structures used in basic research. For deeper structures dry etching is a more feasible method, but the material choices are then more limited. The presented applications include structures for second harmonic generation, filtering, surface plasmon coupling and mass fabrication.

Universal Decimal Classification: 53.084.85, 535.3, 535.4, 681.7.02
PACS Classification: 07.60.-j, 42.70.-a, 42.79.-e, 81.16.-c
Keywords: optics; micro-optics; optical elements; microfabrication; nanofabrication; metals; electron beam lithography; etching; optical harmonic generation; optical filters; surface plasmons

Preface

I wish to thank my supervisors Prof. Jari Turunen and Prof. Markku Kuittinen for guiding me throughout my scientific career and the former head of the Department of Physics and Mathematics, Dean Prof. Timo Jääskeläinen, for offering me the possibility to work first at InFotonics Center and later in our ever-changing department.

Special thanks to Konstantins Jefimovs, Marko Honkanen, Samuli Siitonen and Juha Pietarinen who have taught me everything from the fabrication of micro- and nanostructures to good cleanroom practice. I wish also to thank Benfeng Bai and Anni Lehmuskero for productive co-operation. I am grateful to all my co-authors and project partners outside Joensuu, especially to Brian K. Canfield, Hannu Husu, Jukka Viheriälä, Tero Pilvi and Matti Kaipiainen.

When doing (top-level) research, it is once in a while necessary to have an intermission to clear your head and rest, and what could be a better way to do it than to sit down for a cup of coffee with colleagues whom I value also as friends. Therefore the members of our afternoon coffee break group, Petri Karvinen, Ismo Vartiainen, Ville Kontturi, Kalle Ventola and Jussi Rahomäki, deserve special thanks. All the other past and present members of the Photonics group are also acknowledged.

I am deeply indebted to my reviewers, Prof. Jens Gobrecht and Docent Ari Tervonen, for their valuable comments regarding this manuscript. Personal grants from Foundation of Technology and Emil Aaltonen Foundation are gratefully acknowledged.

I wish to express my gratitude to my parents, Tuula and Keijo, for their support through all my studies. Finally, my deepest and warmest thanks are dedicated to my lovely wife Paula and my children Ella and Aapo for giving me joy and a purpose in life.

Joensuu September 2, 2010 *Janne Laukkanen*

Contents

1 INTRODUCTION 1

2 ELECTROMAGNETIC THEORY FOR METALS 5
2.1 Principles of electromagnetic theory 5
2.2 Optical properties of metals 7
2.2.1 Plasmons 9
2.2.2 Nonlinear optics 10
2.2.3 Effect of surface quality 11
2.3 Computation methods 13

3 ELECTRON BEAM LITHOGRAPHY 15
3.1 Principles of electron beam patterning 15
3.2 Electron beam lithography tools 18
3.2.1 Leica LION-LV1 19
3.2.2 Vistec EBPG5000+ES HR 20
3.3 Resists 20
3.3.1 PMMA 22
3.3.2 ZEP 22
3.3.3 HSQ 23

4 FABRICATION METHODS 25
4.1 Lift-off process 25
4.1.1 Metal deposition 27
4.1.2 Lift-off 30
4.2 Dry etching 31
4.2.1 Argon sputter etching 32
4.2.2 Reactive ion etching 33
4.2.3 Reactive ion beam etching 38
4.2.4 Effect of mask quality 39
4.3 Electrochemical deposition 41
4.4 Atomic layer deposition 44

5 APPLICATIONS FOR METALLIC MICRO- AND NANOSTRUCTURES 47
5.1 Second harmonic generation 47
5.2 Enhanced or suppressed transmission 50
5.3 Polarization rotation 54
5.4 Asymmetrical excitation of surface plasmon polaritons 56
5.5 Mass fabrication 58

6 CONCLUSIONS 61

REFERENCES 63

1 Introduction

Fabrication of micro- and nano-sized structures, latter also referred as nanotechnology, requires highly specialized methods and equipment. Since the structure sizes are smaller than the usual dust particles in the normal room air, the fabrication has to be done in a cleanroom environment. Because of these requirements the establishment of a research environment is very expensive. For the society these labs are essential. To get new commercial applications to the market, the ideas have to be first tested and prototyped. Also basic research is needed to get the new ideas in the first place. For most companies it is financially impossible or at least unwise to build own labs for prototyping and therefore they turn to universities and other research labs with their needs for applied research and development. Careful documentation of the developed processes is needed to pass the information on to the next researcher facing a similar task.

Metallic micro- and nanostructures have become a very popular field of optics research. Plasmonics [1–3] is the umbrella under which the research on the interaction of electromagnetic radiation with metals is placed. Terms like negative refractive index [4–7] and metamaterials [6, 8–10] have been used to depict the extraordinary optical effects which arise from the conductivity of the metals. Whether these terms are appropriate or not is under discussion. Despite this controversy metallic structures have also found numerous applications for example in biosensing [11,12], spectroscopy [13–15] and lasing [16, 17].

To realize the optical effect predicted by theoretical simulations the fabricated structure needs to have same feature sizes as used in the simulation. Controllable fabrication of the metallic micro- and nanostructures is not self-evident. One way of producing metal nanoparticles is to use synthesis but in that case the particles are in colloids [18, 19]. To form structures from individual particles in

colloids one has to use special methods and still the shapes of the structures are limited [20–22]. On the other hand the structure sizes can be smaller than with any other method.

In some cases researchers in the field of optics have used random methods in the fabrication of nanostructures on dielectric substrates [23–25]. This is acceptable in basic research if one can isolate the optical response of the one or few particles of the right size from the overall optical response of the sample, or if the collective response of randomly spaced particles is what the researcher is looking for. However, for large scale commercial exploitation structures cannot be done this way. To be able to use metallic micro- and nanostructures in a repeatable manner in applications their feature sizes have to be tightly controllable.

There are ways of fabricating metallic micro- and nanostructures with precisely defined feature sizes and spacing and some of those methods form the content of this thesis. Before proceeding to fabrication it is wise to simulate the optical response of the structure to avoid useless work in the fabrication. Simulations are based on the electromagnetic theory which is considered in chapter 2 from the point of view of metals. The purpose of the chapter is to give background to the research done with the fabricated structures rather than to cover the whole electromagnetic theory for metals.

Chapter 3 deals with electron beam lithography (EBL) starting from principles. The EBL systems used in this work are presented as well as electron beam resists. Chapter 4 introduces the fabrication methods which have been used to transform the patterns in resist to metal structures. Most of the processes have been used to fabricate structures presented in the next chapter and the rest are described because of their potential. This chapter aims to give the reader pieces of advice to successful fabrication of metal structures and insight into the influence of different fabrication methods on the final outcome of the fabrication process.

The use of fabrication methods in this has work been application oriented. Some of those applications of the metallic structures are presented in chapter 5. They represent the variety of research in the

field of plasmonics and other applications for metallic structures well. The results of the chapter have been previously published in the following papers:

1. Brian K. Canfield, Hannu Husu, Janne Laukkanen, Benfeng Bai, Markku Kuittinen, Jari Turunen and Martti Kauranen, "Local Field Asymmetry Drives Second-Harmonic Generation in Noncentrosymmetric Nanodimers," *Nano Letters* **7,** 1251–1255 (2007).

2. Brian K. Canfield, Sami Kujala, Hannu Husu, Martti Kauranen, Benfeng Bai, Janne Laukkanen, Markku Kuittinen, Yuri Svirko and Jari Turunen, "Local-field and multipolar effects in the second-harmonic response of arrays of metal nanoparticles," *Journal of Nonlinear Optical Physics & Materials*, **16,** 317–328 (2007).

3. Hannu Husu, Brian K. Canfield, Janne Laukkanen, Benfeng Bai, Markku Kuittinen, Jari Turunen and Martti Kauranen, "Local-field effects in the nonlinear optical response of metamaterials," *Metamaterials*, **2,** 155–168 (2008).

4. H. Husu, B. K. Canfield, J. Laukkanen, B. Bai, M. Kuittinen, J. Turunen and M. Kauranen, "Chiral coupling in gold nanodimers," *Applied Physics Letters*, **93,** 183115 (2008).

5. Konstantins Jefimovs, Janne Laukkanen, Tuomas Vallius, Tero Pilvi, Mikko Ritala, Tomi Meilahti, Matti Kaipiainen, Marcos Bavdaz, Markku Leskelä and Jari Turunen, "Free-standing inductive grid filter for infrared radiation rejection," *Microelectronic Engineering*, **83,** 1339–1342 (2006).

6. Benfeng Bai, Janne Laukkanen, Anni Lehmuskero, Xiaowei Li and Jari Turunen, "Polarization-selective window-mirror effect in inductive gold nanogrids," *Physical Review B*, **81,** 235423 (2010).

7. Benfeng Bai, Janne Laukkanen, Anni Lehmuskero, Jari Turunen, "Simultaneously enhanced transmission and artificial

optical activity in gold film perforated with chiral hole array," *Physical Review B*, **81,** 115424 (2010).

8. Benfeng Bai, Xiangfeng Meng, Janne Laukkanen, Tristan Sfez, Libo Yu, Wataru Nakagawa, Hans Peter Herzig, Lifeng Li and Jari Turunen, "Asymmetrical excitation of surface plasmon polaritons on blazed gratings at normal incidence," *Physical Review B*, **80,** 035407 (2009).

9. Juha Pietarinen, Samuli Siitonen, Noora Tossavainen, Janne Laukkanen and Markku Kuittinen, "Fabrication of Ni-shims using UV-moulding as an intermediate step," *Microelectronic Engineering*, **83,** 492–498 (2006).

In the papers 1-4, 6 and 7 the author has planned and executed the fabrication of the studied elements. In papers 5 and 8 the author has done most of the fabrication work of the elements and in paper 9 the author has participated in the electroforming step. In papers 6-8 the author has participated also in the planning of the research. In all papers the author has participated in the writing of parts considering the fabrication. In this thesis the listed papers are referred as [26–34], respectively. Other papers the author has contributed are [35, 36]. They discuss mainly dielectric structures.

2 Electromagnetic theory for metals

The topic of this thesis is the fabrication of nano- and micro-sized metal structures for optical solutions. Despite the experimental nature of the work, a brief coverage on the interaction of electromagnetic fields with metals is needed. Without a way to predict the optical response of the considered structure one could waste a lot of time and effort in the fabrication of an element which would turn out to be useless. The analysis of interaction between the electromagnetic fields and diffractive optical elements with conductive parts requires more computation than with purely dielectric elements. The limits of computational power are diminishing through the constant development of computers, but still in some cases the convergence of the simulation is uncertain. On the other hand it can be hard to fabricate structures with exactly the same parameters as in the design. Therefore it is often said that it's hard to get the theoretical and experimental results to match. In a few cases described in chapter 5 an almost perfect match is achieved.

In this chapter the principles of electromagnetic theory and optical properties of metals are briefly considered. In the last section the computation methods for analyzing the optical response of metal structures are described.

2.1 PRINCIPLES OF ELECTROMAGNETIC THEORY

The macroscopic Maxwell's equations are the fundamental starting point for the analysis of the electromagnetic response of a medium. They describe the relations of the electric field $\boldsymbol{E}(\boldsymbol{r},\omega)$ to the magnetic induction $\boldsymbol{B}(\boldsymbol{r},\omega)$, and the magnetic field $\boldsymbol{H}(\boldsymbol{r},\omega)$ to the electric current density $\boldsymbol{J}(\boldsymbol{r},\omega)$ and the electric displacement $\boldsymbol{D}(\boldsymbol{r},\omega)$. Because of the significant frequency dependence of the optical re-

sponse of metals the equations are written in the following form

$$\nabla \times \boldsymbol{E}(\boldsymbol{r},\omega) = \mathrm{i}\omega \boldsymbol{B}(\boldsymbol{r},\omega)\ , \tag{2.1}$$

$$\nabla \times \boldsymbol{H}(\boldsymbol{r},\omega) = \boldsymbol{J}(\boldsymbol{r},\omega) - \mathrm{i}\omega \boldsymbol{D}(\boldsymbol{r},\omega)\ , \tag{2.2}$$

$$\nabla \cdot \boldsymbol{D}(\boldsymbol{r},\omega) = \rho(\boldsymbol{r},\omega), \tag{2.3}$$

$$\nabla \cdot \boldsymbol{B}(\boldsymbol{r},\omega) = 0\ , \tag{2.4}$$

where ω is the angular frequency and $\rho(\boldsymbol{r},\omega)$ the electric charge density. If we assume our material to be linear and isotropic we have the constitutive relations

$$\boldsymbol{D}(\boldsymbol{r},\omega) = \epsilon_0 \epsilon_r(\boldsymbol{r},\omega)\boldsymbol{E}(\boldsymbol{r},\omega)\ , \tag{2.5}$$

$$\boldsymbol{B}(\boldsymbol{r},\omega) = \mu_0 \mu_r(\boldsymbol{r},\omega)\boldsymbol{H}(\boldsymbol{r},\omega)\ , \tag{2.6}$$

$$\boldsymbol{J}(\boldsymbol{r},\omega) = \sigma(\boldsymbol{r},\omega)\boldsymbol{E}(\boldsymbol{r},\omega)\ , \tag{2.7}$$

where ϵ_0 and μ_0 are the electric permittivity and magnetic permeability of vacuum and ϵ_r, μ_r and σ are the relative permittivity (also called the dielectric function), permeability and conductivity, respectively. In this work only nonmagnetic materials are used, thus $\mu_r = 1$. Polarization $\boldsymbol{P}(\boldsymbol{r},\omega)$ is the electric dipole moment per unit volume inside the material, caused by the alignment of the microscopic dipoles with the electric field. Polarization is related to the internal electric charge density by $\nabla \cdot \boldsymbol{P}(\boldsymbol{r},\omega) = -\rho(\boldsymbol{r},\omega)$. Introducing the dielectric susceptibility χ we get

$$\boldsymbol{P}(\boldsymbol{r},\omega) = \epsilon_0 \chi \boldsymbol{E}(\boldsymbol{r},\omega). \tag{2.8}$$

The electric permittivity $\epsilon_r(\omega) = \epsilon_1(\omega) + \mathrm{i}\epsilon_2(\omega)$ and the conductivity $\sigma(\omega) = \sigma_1(\omega) + \mathrm{i}\sigma_2(\omega)$ of a uniform medium are complex functions of angular frequency. The complex refractive index of the medium is given by

$$\hat{n}(\omega) = \sqrt{\hat{\epsilon}_r(\omega)} = n(\omega) + \mathrm{i}\kappa(\omega), \tag{2.9}$$

where

$$\hat{\epsilon}_r(\omega) = \epsilon_r(\omega) + \mathrm{i}\frac{\sigma(\omega)}{\omega\epsilon_0}. \tag{2.10}$$

n is called the refractive index and κ the extinction coefficient of the medium.

From the equations above we can derive the *Helmholtz equation*

$$\nabla^2 \boldsymbol{E} + k_0^2 \hat{\epsilon}_r(\omega) \boldsymbol{E}(\boldsymbol{r}, \omega) = 0, \tag{2.11}$$

where k_0 is the wave vector of the propagating wave in vacuum. The solutions of the equation (2.11) are the propagating and evanescent waves of the system [37].

2.2 OPTICAL PROPERTIES OF METALS

When studying the optical responses of metals, a perfect conductivity of the material is many times assumed for simplicity. In perfect conductor the flow of electrons is completely free and therefore the resistance of the material is zero. Also there cannot be an electric field parallel to the surface. This assumption allows an analytic solution of the modes of the optical field, but the solutions might be inaccurate at optical frequencies.

In plasma model the optical properties of metals are depicted by considering the optical response of a free electron gas in an electric field. In the plasma model the gas of free electrons (electron concentration N) moves against a fixed background of positive ion cores [38]. This model can be well used for alkali metals in the visible frequencies but for noble metals it is not accurate because of the interband transitions. Details of lattice potential and electron-electron interactions are ignored. The applied electric field oscillates the electrons and their movement is attenuated by collisions occurring with a characteristic frequency $\gamma = 1/\tau$, where τ is the relaxation time of the free electron gas. Plasma frequency of the free electron gas is given by

$${\omega_p}^2 = \frac{Ne^2}{\epsilon_0 m_\mathrm{e}}, \tag{2.12}$$

where m_e is the effective mass of the electron. In table 2.1 empirical plasma frequencies for thin films of gold, silver, copper [39] and

Table 2.1: Empirical plasma frequencies for thin films of gold, silver, copper [39] and aluminum [40].

material	ω_p $[s^{-1}]$
Au	13.8×10^{15}
Ag	14.0×10^{15}
Cu	13.4×10^{15}
Al	13.5×10^{15}

aluminum [40] are listed. The dielectric function of the free electron gas can then be written in the form

$$\epsilon(\omega) = 1 - \frac{{\omega_p}^2}{\omega^2 + \mathrm{i}\gamma\omega}, \tag{2.13}$$

which is also known as the *Drude model* of the optical response of metals [41]. The components of the complex dielectric function $\epsilon(\omega) = \epsilon_1(\omega) + \mathrm{i}\epsilon_2(\omega)$ can be calculated from

$$\epsilon_1(\omega) = 1 - \frac{\omega_p^2\tau^2}{1 + \omega^2\tau^2}, \tag{2.14}$$

$$\epsilon_2(\omega) = \frac{\omega_p^2\tau}{\omega(1 + \omega^2\tau^2)}. \tag{2.15}$$

In reality the electric field can penetrate the metal surface. Due to the atomic structure of metals the current density is highest at the surface and it gradually diminishes when we go deeper into the metal. When electromagnetic radiation penetrates the metal its amplitude is then also gradually damped. When the amplitude has decreased to $1/e$ of its surface value it has reached a distance called the *skin depth*. Skin depth is given by

$$\delta = \frac{c}{\kappa\omega} = \sqrt{\frac{2}{\sigma_0\omega\mu_0}}, \tag{2.16}$$

where σ_0 is the dc-conductivity of the material. From (2.16) we can see that the skin depth is smaller for better conductors.

2.2.1 Plasmons

Collective oscillations of the conduction electrons are called plasmons. There are three different types of plasmons, each with their own characteristic nature; volume plasmons inside the metal, surface plasmon polaritons propagating at the metal-dielectric interface and non-propagating localized surface plasmons.

Volume plasmons are longitudinal oscillations inside the metal. Volume plasmons do not couple to transverse electromagnetic waves because of the longitudinal nature of excitation and they can be excited only by particle impact. Their energy is reduced by Landau damping. [38]

Surface plasmons are electron oscillations at the metal surface. A combined excitation consisting of a surface plasmon and a photon is called a surface plasmon polariton (SPP) [42]. The dispersion relation of a SPP on a smooth metal surface is given by [43]

$$k_{\mathrm{SPP}} = k\sqrt{\frac{\epsilon_{\mathrm{met}}\epsilon_{\mathrm{die}}}{\epsilon_{\mathrm{met}} + \epsilon_{\mathrm{die}}}} \equiv k\hat{\delta}, \tag{2.17}$$

where $k = \omega/c$ is the light wave number in vacuum, and ϵ_{met} and ϵ_{die} are the permittivities of the metal and adjacent dielectric, respectively. If ϵ_{met} is complex, the wave number k_{SPP} is also complex and we can write

$$k_{\mathrm{SPP}} = k_{\mathrm{SPP}}^{(r)} + \mathrm{i}k_{\mathrm{SPP}}^{(i)}. \tag{2.18}$$

The field is confined to the surface since the propagation constant k_{SPP} is greater than the wave vector k in the dielectric. Therefore the field is evanescent on both sides of the interface. The wavelength of the surface plasmon polariton can be defined as

$$\lambda_{\mathrm{SPP}} = \frac{2\pi}{k_{\mathrm{SPP}}^{(r)}} = \frac{\lambda}{\Re\{\hat{\delta}\}} = \lambda\Re\sqrt{\frac{\epsilon_{\mathrm{met}} + \epsilon_{\mathrm{die}}}{\epsilon_{\mathrm{met}}\epsilon_{\mathrm{die}}}}, \tag{2.19}$$

where $\lambda = 2\pi/k$ is the vacuum wavelength of light and $\Re$ denotes the real part.

Since the SPP dispersion curve always lies on the right side of the light line $k = \omega/c$ without crossing it [38], a SPP cannot couple

to a radiative mode and, conversely, cannot be directly excited by light propagating in the dielectric. However, if a grating with period d in x-direction is introduced, momentum conservation can be satisfied through the mth evanescent diffraction order by

$$|k_x + mK\hat{x}| = \frac{\omega}{c}\Re\{\hat{\delta}\}, \tag{2.20}$$

where $k_x = |\boldsymbol{k_x}| = k \sin\theta$, θ is the angle of incidence and $K = 2\pi/d$. With two-dimensionally periodic structure the excitation condition for surface plasmons is

$$|k_x + mK_x\hat{x} + nK_y\hat{y}| = \frac{\omega}{c}\Re\{\hat{\delta}\}, \tag{2.21}$$

where $K_x = 2\pi/d_x$, $K_y = 2\pi/d_y$, d_x and d_y are the periods in x and y directions, respectively, and m and n are integers.

It has been proposed that plasmonic waveguides and switches could be used to make an optical transistor and through it an optical processor [2]. This approach is replacing the idea of using photons in processors since the size of the waveguides and other needed elements can be a smaller. In these speculations it is unfortunately forgotten that the evanescent tail of the SPP in the dielectric side is long and some kind of barriers are needed between closely placed waveguides.

Localized surface plasmons (LSPs) are non-propagating excitations of conduction electrons of metallic nanostructures coupled to the electromagnetic field [38]. They arise from the scattering problem of a small, subwavelength conductive nanoparticle in an oscillating electromagnetic field. Electrons are pulled back to the particle surface by a force arising from the curvature of the particle allowing a resonance to occur leading to field enhancement both inside and in the near field outside the particle. Contrary to the surface plasmon polaritons, localized surface plasmons can be excited by a direct light illumination.

2.2.2 Nonlinear optics

In nonlinear optics the optical properties of a material system are modified by the presence of light [44]. Typically, only laser light has

enough intensity to evoke such phenomena. Nonlinearity in this case means that the response of the material system depends on the strength of the optical field. The most classic nonlinear optical phenomenon is second harmonic generation [45]. In second harmonic generation nonlinear material is illuminated with a monochromatic light beam, wavelength λ. The emerging radiation contains the original wavelength, but also radiation with doubled frequency, i.e. wavelength $\lambda/2$.

The nonlinearity of the material system is caused by the dipole moment per unit volume, or polarization $P(t)$ [44]. It depends on the strength $E(t)$ of the applied optical field. Polarization of the material system can be written as a power series

$$P(t) = \chi^{(1)}E(t) + \chi^{(2)}E^2(t) + \chi^{(3)}E^3(t) + \cdots \quad (2.22)$$

$$= P^{(1)}(t) + P^{(2)}(t) + P^{(3)}(t) + \cdots, \quad (2.23)$$

where $\chi^{(2)}$ and $\chi^{(3)}$ are the second- and third-order nonlinear optical susceptibilities, respectively. For simplicity the fields $P(t)$ and $E(t)$ are here taken as scalar quantities. For vector approach reader is advised to check reference [44].

2.2.3 Effect of surface quality

It has been found that thin metal films have different optical properties than bulk metals [46]. The optical properties depend on the thickness of the film and on the used deposition technique. The affecting parameters are grain size and porosity of the material. There might also be some impurities like oxides in the material caused by the deposition conditions. With very small structures like gratings the surface area of the structure is large compared to the volume of the element. Therefore the effective refractive index is largely affected by the surface quality.

To get the simulations and experimental results match it is better to use refractive index measured from a film with similar thickness and the same deposition technique. In figures 2.1 and 2.2 three different refractive index and extinction coefficient graphs are shown

for gold. Values for bulk material have been taken from [47] and values for 40 nm and 100 nm thick evaporated films were measured by ellipsometry.

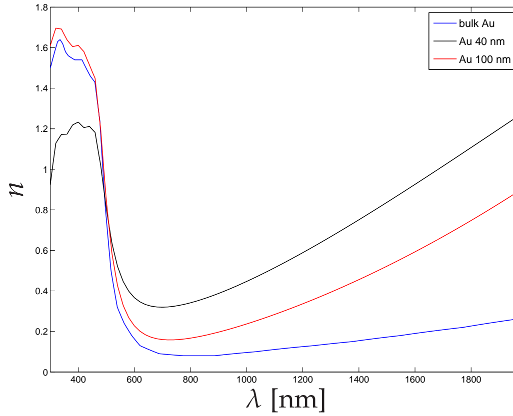

Figure 2.1: Three refractive index graphs for gold. Values for bulk gold are taken from [47] and values for thin films are measured by ellipsometry (courtesy of Anni Lehmuskero).

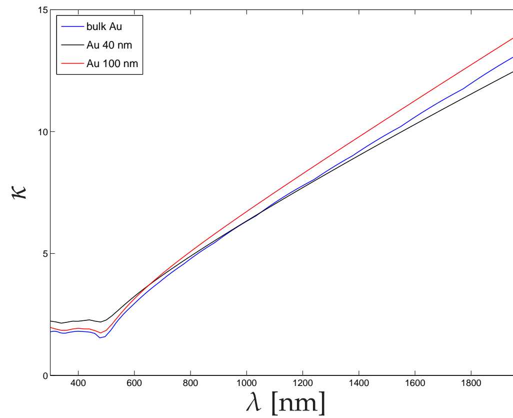

Figure 2.2: Three extinction coefficient graphs for gold. Values for bulk gold are taken from [47] and values for thin films are measured by ellipsometry (courtesy of Anni Lehmuskero).

2.3 COMPUTATION METHODS

The simulation of the optical response of metallic micro- and nanostructures is more demanding than of dielectrics because of the conductivity. If we assume the conductivity to be infinite the simulation is a bit easier because then we can neglect the electric field parallel to the metal surface. This however is not true for real metals in the optical region and more reliable results are gotten if finite conductivity is taken into account [48]. Analytical solutions are then not available and one has to use numerical methods in simulations. The structures analyzed in this work are periodic and thus the optical fields they produce consist of propagating and evanescent diffraction orders. When analyzing the optical response of a micro- or nanostructure with methods based on the use of Fourier series one has to take enough diffraction orders into calculation to get the series to converge. Unfortunately when the finite conductivity of the structure is taken into account the memory requirement and computation time increase heavily.

Many different computational methods have been developed to get as accurate simulations as possible. Methods like boundary element method (BEM) [49], discrete dipole approximation (DDA) [50] and finite-difference time-domain method (FDTD) [51, 52] are widely used. In our simulations we have used Fourier modal method (FMM) [53–56]. FMM is a simple and versatile method for simulations. With symmetry considerations computational efficiency can be greatly improved and thus we can take more diffraction orders into simulation, leading to better convergence of the Fourier series [57].

3 Electron beam lithography

Electron beam lithography (EBL) is a technique for creating extremely small patterns in resist. It was originally developed for the electronics industry [58], but has found use also in optics [59, 60]. Compared to optical lithography [61, 62] the resolution of the electron beam patterning tools is far better. As small as 10 nm feature sizes have been reported [63, 64]. Also the patterns can be more complex and there are less restrictions for the substrate. On the down side the tools are expensive and relatively slow. In the research environment the flexibility of the technique is invaluable.

In this chapter first the principles of electron beam patterning are described. In the second section the electron beam lithography tools used in this work are presented. In the last section the used electron beam resists are described.

3.1 PRINCIPLES OF ELECTRON BEAM PATTERNING

In electron beam lithography the patterns are generated in a high-energy sensitive material, resist, on a substrate by scanning the surface with a beam of electrons. The first EBL tools were made from scanning electron microscopes in the late 1960s. The electron beam is formed in the column of the EBL system [58]. In figure 3.1 a schematic of the column in the Vistec EBPG5000+ES HR electron beam lithography tool is presented. A basic column has an electron source, an alignment system, a blanker, two or more magnetic lenses, a deflector, a stigmator, apertures and an electron detector. The electrons are emitted from the source and are accelerated through the column by applying a voltage. The alignment system centers the beam in the column and the electron lenses focus the beam. Apertures are used to stop any stray electrons and to limit the beam, the blanker to turn the beam on and off and the deflector to scan the beam on the sample surface. The stigmator is

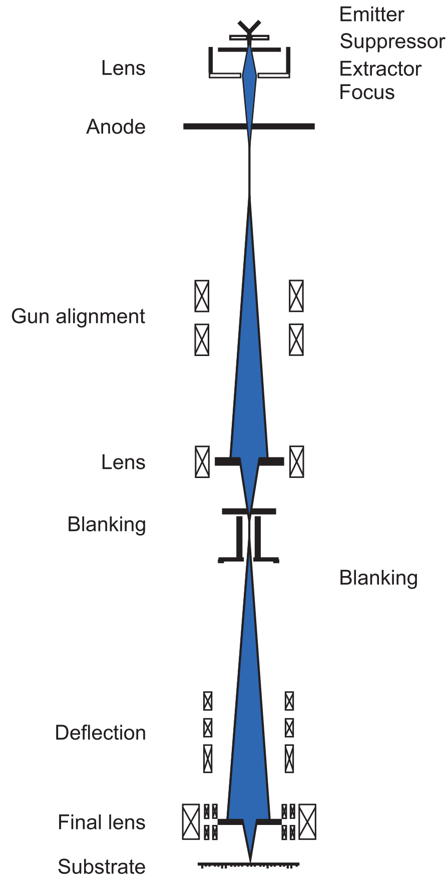

Figure 3.1: Schematic of the column in the Vistec EBPG5000+ES HR electron beam lithography tool. (Courtesy of Vistec Lithography Ltd.)

used to correct beam astigmatism caused by the imperfections in the construction and alignment of the column. Electron detector helps in the focusing of the beam and finding the alignment marks. Since the beam can be deflected only on a small area without compromising the accuracy, the sample is placed on a motorized, high precision x–y table in a chamber located underneath the column to enable patterning on the whole sample area. A vacuum system is needed to provide suitable environment inside the column and chamber and a loading system to move the sample in and out [58].

The place of some elements, like the beam blanking unit for example, can vary between columns made by different manufacturers.

There are plenty of different EBL systems on the market. Gaussian beam shape systems give the smallest spot size but the throughput of the systems is not good enough for mainstream very-large-scale integration (VLSI) manufacturing. However for academic research and industrial research and development Gaussian beam systems are the most common choice. Variable shaped beam systems give more throughput, but resolution is worse than with Gaussian beam systems. To increase throughput new electron beam system types, such as electron projection and parallel maskless systems, have been developed [65], but so far they are not very widely used.

Electron beam pattering is done to a resist layer on top of a substrate. Resist is a high-energy sensitive material which is usually dissolved in a liquid solvent and therefore it can be spread on the sample by spinning or spraying. Usually the remains of the solvent are baked away after the coating. The energy of the electron beam alters the molecular structure of the resist material in a way that either the altered (positive resist) or the unaltered material (negative resist) can be diluted away with a developer solution [58].

One can design any kind of pattern to be exposed, but many factors affect the final dimensions of the developed pattern. Exposure parameters, beam properties, resist properties and electron-solid interactions are the most influential. Beam current and the exposure dose are system parameters the user can (within system limits) define. Spot size is the result of the combination of user defined parameters, column properties and alignment [66,67]. Higher operating voltage leads to a smaller spot size. The achievable resolution however is not limited by the spot size but by the electron scattering. The scattered electrons in solids can be divided to forward scattered electrons (scattering angle less than 90°) and backscattered electrons (scattering angle approaching 180°). At low doses the line width is influenced mostly by the forward scattered electrons. At higher doses backscattering starts to have more influ-

ence. Higher beam energy and low dose results in less scattering and therefore smaller line width [68]. Backscattering causes also a phenomenon called the proximity effect [69,70]. The backscattering range, i.e. the maximum length the electrons travel in the layers under the resist before scattering back to the resist layer, of high energy electrons is in most cases wider than the exposed line. Therefore the neighboring lines get also some energy and are widened. Total dose is smaller for the lines near the edges of the pattern than for the lines in the center. That leads to different line widths. Because of the fundamental nature of the problem, hundreds of researchers have studied the proximity effect after the first experiments in electron beam lithography and several different correction methods have been developed [71,72].

Besides the positive/negative classification of resists, they can also be divided by the aimed resist profile after development. Binary resist aim to two level profiles and analog resists to continuous profiles. Sensitivity and resolution are the most important binary resist properties. Sensitivity gives the minimum dose required for the pattern to be developed. Resolution tells the smallest achievable feature size for the used resist [73]. For analog resists there are more choices in the market and the aimed profile defines the desired resist properties. Usually analog resists are used as a lot thicker layers than binary resists and therefore forward scattering inside the resist has a bigger effect to the resolution.

3.2 ELECTRON BEAM LITHOGRAPHY TOOLS

The main requirements for the EBL systems are critical dimensional control, alignment accuracy, cost-effectiveness, flexibility and compatibility with other exposure tools [73]. The two EBL systems used in this work, Leica LION LV1 and Vistec EBPG5000+ES HR fulfil these requirements very well. Both are Gaussian beam systems with a very high accuracy and a small spot size.

3.2.1 Leica LION-LV1

The Leica LION-LV1 is a Gaussian beam vector scan EBL system from Leica Lithographie Systeme Jena GmbH. The LION has a column from ICT GmbH (Heimstetten, Germany) and a pattern generator from Raith GmbH. The column is shown in figure 3.2. The electron source is thermal field emitter (TFE). The system has two operating modes: Step-and-go and continuous path control. In the step-and-go mode the pattering is done by vector scanning. In vector scanning the pattern is split to mainfields which are further split to subfields. The beam is scanned across one subfield at a time for the whole mainfield area and then the sample is moved by the table for the next main field to be patterned. In the continuous path control the beam is held close to the center of the field and the pattern defined by moving the table [58].

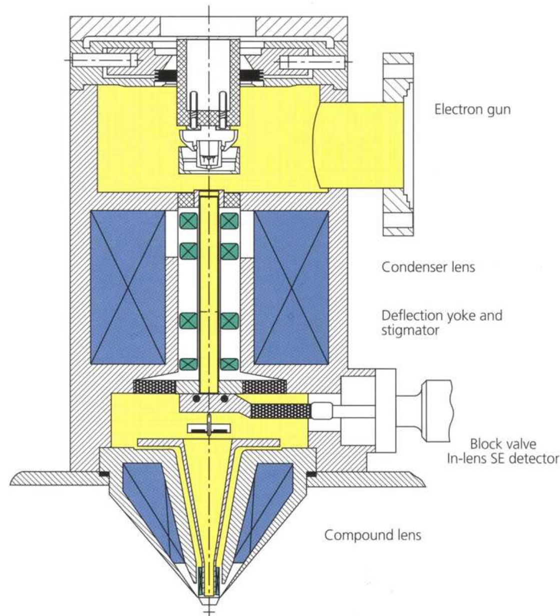

Figure 3.2: Column of the Leica LION-LV1 electron beam lithoragpy tool. (Courtesy of Vistec Lithography Ltd.)

LION-LV1 has an operating voltage range of 1–20 kV so it can be used as a low voltage system or as regular, high beam energy EBL. With low voltage the proximity effect and substrate damage can be avoided [58]. Low voltage combined with continuous path control enables making of curved structures with smooth edges [74]. In this work operating voltage of 15 kV was used to achieve better penetration through the relatively thick resist layers. In the vector scanning mode the maximum working field size can be 180 μm $\times$ 180 μm. The system has an autoloader with the maximum capacity of 13 substrate holders. Substrates can be mask plates, wafers or piece parts. Maximum mask plate size is 5″ and maximum wafer size 150 mm. The system is not in our use anymore since it was replaced by the Vistec EBPG5000+ES HR.

3.2.2 Vistec EBPG5000+ES HR

The Vistec EBPG5000+ES HR is a cheaper and somewhat simpler version of the full Vistec EBPG5000+ EBL tool. The ES stands for entry system and HR for high resolution. The core features are the same as in full EBPG5000+ system and by a series of upgrades the performance of a full system can be achieved. This Gaussian beam vector scanning system can operate with 50 kV or 100 kV voltage and the minimum spot size is less than 2.5 nm. The electron source is a high current density thermal field emission gun. The pattern generator of our system has been upgraded to work with up to 50 MHz frequency making the exposures really fast compared to the LION LV-1. With 50 kV operating voltage the maximum working field size is 409.6 μm $\times$ 409.6 μm and with 100 kV it is 256 μm $\times$ 256 μm. The system has a 2-holder airlock and specific holders for different substrates ranging from very small piece parts up to 6″ mask plates.

3.3 RESISTS

Electron beam resists are materials sensitive to the energy of the electron beam. The chemistry of the resist defines the relationship

of the absorbed energy to the change of the molecular weight of the resists and the influence of the developer [69]. Typically in electron beam lithography the energy of the electrons is 10–100 keV, but also lower and higher energies have been used. Since EBL is used for many different purposes also the desired properties of the resists vary. Usually high resolution and high sensitivity are the most sought properties, but when we want to transfer the resist pattern to the substrate, etch resistance of the material might be more important. The continuous research on new resist materials and development chemistries has lead to a wide variety of commercially available resists and developers.

Resists are dissolved in a liquid solvent and in most cases they are spread on a substrate by spin coating, because it is the most reproducible method. Other coating techniques such as spray, roll and dip coating are also used, but they produce less uniform layers. After spreading the resist the solvent is removed by softbake (also called prebake). Softbake affects the outcome of the exposure and development and therefore the baking should be done carefully, keeping the conditions and procedure constant [73].

After electron beam exposure the pattern in the resist is brought out in development. The resist is developed by immersion, spray or puddle method. Immersion development can be done simply in any chemical resistant vessel, but spray and puddle development methods require dedicated equipment. Since the latter two are automated processes, their reproducibility is better.

Resists are divided to two groups by their response to the energy of the electrons: those which are more soluble to the developer liquid after the irradiation are called positive and those which get less soluble are called negative. In general positive resists are used for making binary profiles [68] and negative resists for making continuous profiles [75], but there are also some exceptions. One can make continuous profiles with positive resist [76] and binary profiles with negative resist [77]. In this work only binary profiles have been made and therefore only resists suitable for such fabrication processes are discussed in this section.

3.3.1 PMMA

Although invented by Haller and coworkers already in the year 1968 [78], polymethyl methacrylate (PMMA) is still a very widely used positive resist. It is a high resolution polymeric resist and during the electron beam irradiation the long PMMA chains are fragmented into shorter ones. Shorter chains are dissolvable for the developer, typically methyl isobutyl ketone (MIBK). PMMA is sold in many different molecular weights and it is dissolved in chlorobenzene, ethyl lactate or anisole. For isolated lines, higher molecular weight provides better line-to-line resolution, but for dense gratings the high molecular weight resists tend to swell in developer and thus limit the grating development [79]. The contrast and sensitivity of the PMMA resist can be adjusted by changing the strength of the developer with the addition of isopropanol (IPA). With a 1:3 MIKB:IPA solution a very high contrast can be achieved, but the sensitivity is low. Using 1:1 MIBK:IPA solution gives a lot better sensitivity with a small loss of constrast [58]. The smallest reported lines patterned in PMMA are less than 5 nm wide [80, 81]. PMMA is not a very good mask material for plasma etching, because it is etched away quite easily. On the other hand for lift-off process (described in section 4.1) it is the first choice.

PMMA resist used in this work was AR-P 661 (Allresist GmbH). It has a molecular weight of 600K and is dissolved in chlorobenzene. The samples were developed in a 1:2 MIBK:IPA solution for 60 seconds and rinsed with isopropanol for 30 seconds.

3.3.2 ZEP

Another positive resist used in this work was ZEP 7000-22 from Zeon Corporation. It is a methyl styrene/chloromethyl acrylate copolymer and it is dissolved in diglyme (bis(2-methoxyethyl)ether). It has a good resolution and a very high sensitivity. ZEP has an excellent plasma etching resistance making it a good mask material for example in dry etching of metals (described in section 4.2). Zeon corporation sells its own developers ZED-500 and ZED-750 for ZEP

7000-22, but in our tests we found that better quality structures can be achieved using ethyl 3-ethoxypropionate (EEP). EEP gives a little bit better resolution and the remaining resist layer is thicker than with Zeon's own developers. With EEP we used 60 second developing time followed by a 30 second rinse in IPA and after that a rinse under flowing DI water.

3.3.3 HSQ

Hydrogen silsesquioxane, HSQ (FOX-12 Flowable Oxide, Dow Corning Co.) is a high resolution negative resist [82]. It is purely inorganic material and it is dissolved in methyl isobutyl ketone (MIBK). In most cases 0.26N tetramethyl hydroxyl ammonium (TMAH) is used as a developer but also other developers have been proposed [83–85]. In this work Microposit 351 developer was used.

The molecule size of HSQ is very small resulting in smooth line edges even for very narrow lines. Structures with less than 10 nm feature sizes have been done in HSQ [63, 64, 86]. Grigorescu and Hagen have extensively reviewed material properties and current developments of HSQ in Ref. [87]. To summarize one can say that the material can be used as a high resolution negative tone electron beam resist but it also has some limitations. The shelf life of the resist is only 6 months and because of the high sensitivity to contamination it should always be stored at 5 °C and in polyethylene or fluorocarbon bottles. The sensitivity of the resist increases with time but the resolution and contrast are decreased. Also the delay between the prebake and exposure affects the sensitivity of HSQ [88]. However the delay between exposure and development doesn't have any effect on sensitivity or resolution at least when a 2-minute prebake in temperature of 150 °C is used [89]. The removal of HSQ after subsequent process steps requires the use of buffered hydrofluoric acid (BHF) which dilutes also other oxides from the sample. This can be avoided by using acetone-soluble PMMA underlayer below HSQ [90].

HSQ seems to be particularly applicable in the fabrication of

metallic nanoparticles. It could be used as an etching mask for similar structures as the ones presented in section 5.1. However it has been reported that the adhesion of HSQ on gold is not very good [91]. This can be avoided by using proper surface treatment before applying HSQ. In figure 3.3 L-shaped structures made of HSQ resist on a fused silica wafer coated with aluminum are presented.

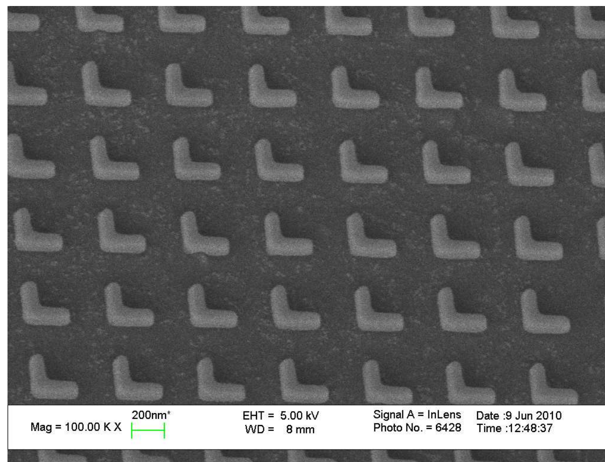

Figure 3.3: L-structures made of HSQ resist.

4 Fabrication methods

After patterning the sample, we are still far from ready. There are multiple ways of turning the pattern in resist to a metal micro- or nanostructure and all of the methods used in this work are presented in this chapter. The most used method of this work, the lift-off process, is described in the first section. Although being an age-old process and well known to experienced readers, the lift-off process is described quite extensively to give a good starting point also to inexperienced readers. Dry etching of metals and dielectrics is described in the second section followed by sections for electroplating and atomic layer deposition (ALD).

4.1 LIFT-OFF PROCESS

Lift-off process is an old method for fabrication of metal micro- and nanostructures. Originally the process has been developed for printed circuit fabrication and at that time the structure sizes were in millimeters [73]. The steps of a typical lift-off process are shown in figure 4.1. First a substrate is covered with a resist which can be patterned for example by electron beam lithography (EBL) [92], photolithography [93], nanoimprint lithography (NIL) [94] or soft interference lithography [95]. In this work we used EBL for patterning. Resist thickness should be at least twice the thickness of the aimed metal structure for successful lift-off.

After development it is crucial to remove any traces of resist from the areas where we want the metal to be attached. This is done by oxygen plasma in a reactive ion etcher. It should be noted that when we are removing the residual resist from the developed areas we are also etching the resist mask. If a too long etching time is used, the mask is thinned and the corners start to get rounded.

In the next step the metal is deposited on the sample. If the used material has poor adhesion to the substrate material (for ex-

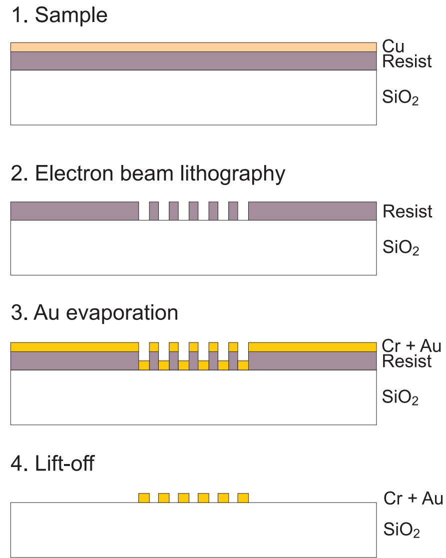

Figure 4.1: The steps of the lift-off process.

ample gold on fused silica), an adhesion promoting layer has to be deposited under the main layer. The metal deposition techniques used in this work are presented in section 4.1.1. In the final step the remaining resist and the metal on top of it are removed, i.e. lifted off by dissolution or swelling (see section 4.1.2). After this step only the metal in contact with the substrate remains.

The most used resist for lift-off process is PMMA because of its good resolution and the easy handling, but also because the dissolution of it can be done by acetone. In the use of PMMA it should be remembered that the material is quite soft and structures with aspect ratio (i.e. the ratio of the height of the structure to its width) over one can lead to bending of the structure. The key to a successful completion of the lift-off process is the correct resist profile after development. In metal deposition the material is mostly applied to the horizontal surfaces but some of it is attached also to the vertical resist walls. This makes the dissolution of resist harder since the liquid cannot get straight in contact with the resist. If there is enough undercut in the resist profile the metal deposition on the

resist walls is not a problem. Another way of getting a suitable resist profile is to use double layer process [96], but for gratings with very narrow lines there is a risk of line collapse.

Lift-off is a simple method for fabricating metal structures. On the down side the structure depth is limited and the success of the process is not certain. Many times there are some areas where the metal structure is lost for some reason and in other areas there might be redeposited metal on top of the structure. All in all for shallow structures for basic research the method is feasible and for gold structures it is the only possible method at this point.

4.1.1 Metal deposition

Metal depositions for lift-off processes carried out in this work have been done by two different techniques; thermal evaporation and sputtering. Both of them have to be done in vacuum or at least in very low pressure [97]. Otherwise the gaseous species of the material to be deposited cannot reach the target substrate. The most used technique was thermal evaporation which is described first. Second technique, used especially for adhesion layer deposition, was sputtering.

Thermal evaporation

In thermal evaporation the substrate and the material source are placed inside a vacuum chamber. We have used two vacuum evaporators for this method: Leybold L560 and Leybold Heraeus Univex 300. In the L560 the chamber is bigger and thus the evaporation distance is larger. It also has bigger vacuum pumps than Univex 300 so it can reach better vacuum. The best achievable vacuum in Univex 300 is around 3×10^{-6} mbar with over night pumping and in L560 it is about one order of magnitude lower. However the L560 has a separate high vacuum sensor and the Univex 300 has not. The pressure 3×10^{-6} mbar is close to the limit of the measurement range of the basic sensor in Univex 300 and the actual pressure might be higher since in the L560 the basic sensor shows lower pressure than

the high vacuum sensor near the limit of its range. On the other hand in the Univex 300 it is possible to place the substrate straight above the thermal source which is not possible in the L560. In some cases the straight deposition angle is critical for the structure profile. Both systems are equipped with Inficon XTC deposition monitors.

Heating of the source material is done either by resistive heating of a tungsten boat or by high energy electron beam. Resistive heating can be less clean than electron beam heating because the boat contacts can also heat up [97]. Electron beam heating can also reach a higher temperature than resistive heating thus making it applicable for a bigger range of materials. For gold deposition the temperature needed is relatively low and since resistive heating is a bit easier to do it has been applied in most cases presented in this thesis.

Because evaporation is a line-of sight deposition technique, there is a thickness gradient on the substrate [97]. This can be avoided by using sample rotation during deposition. The sample is rotated around the chamber which changes the incident angle of the deposited material and therefore averages out the thickness variation. This works well for plain thin films but for lift-off it can be harmful.

The amount of metal deposited on the resist mask walls is then higher which is particularly problematic for small structures. In figure 4.2 the same resist mask (period 200 nm, linewidth 110nm) has been covered with a 30 nm thick layer of evaporated chromium. The sample shown in figure 4.2(a) was rotated during the evaporation and the sample in figure 4.2(b) was placed straight above the evaporation source. The difference in the metal deposition is visible.

Bigger structures don't get buried like smaller ones, but with them the shape of the achieved metal structure is not optimal. In figure 4.3 a resist mask (period 500 nm, linewidth 250 nm) has been covered with a 50 nm thick layer of evaporated chromium. One can see from 4.3(a) that the amount of metal in the sidewalls of the mask is acceptable but the surface of the metal in the grooves

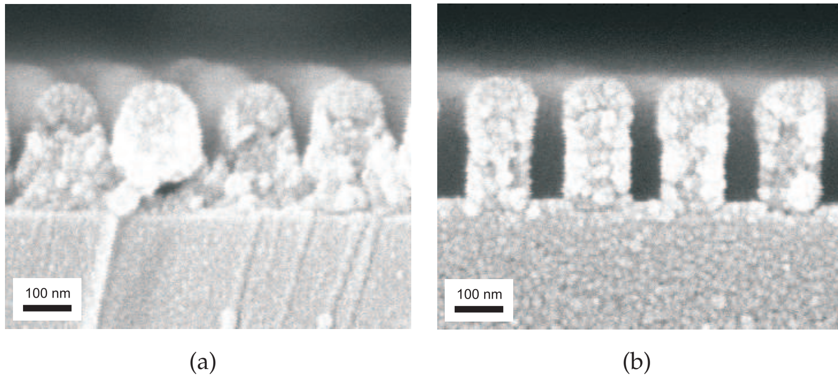

Figure 4.2: Resist mask (period 200 nm, linewidth 110nm) covered with a 30 nm thick evaporated chromium layer. In (a) the sample was rotated during the evaporation and in (b) the sample was placed straight above the evaporation source.

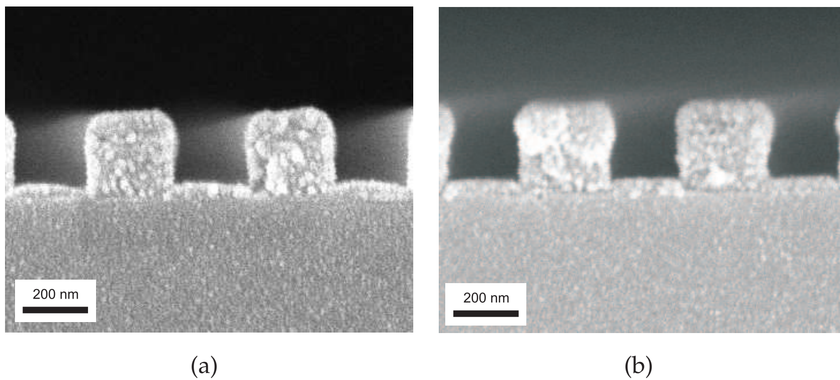

Figure 4.3: Resist mask (period 500 nm, linewidth 250nm) covered with a 50 nm thick evaporated chromium layer. In (a) the sample was rotated during the evaporation and in (b) the sample was placed straight above the evaporation source.

is curved whereas in 4.3(b) the surface is straight. The reason for curved surface is the shadowing of the mask in the evaporation when the sample is rotated. The effect of mask shape is discussed in section 4.2.4.

Sputtering

Sputtering is done in inert gas atmosphere, in most cases in argon [62]. Either DC or RF power supply generates plasma around the target and inert gas ions dislodge ions from the target onto the substrate [97]. DC sputtering can be used to deposit metals but it cannot be used with dielectric materials. RF sputtering can be used for both, but the deposition rate is lower in RF sputtering because there are fewer ions in the plasma. Deposition rate can be improved by adding a strong magnetic field perpendicular to the electric field. Magnetic field ionizes more gas molecules and it is applied by placing magnets below the target. The sputtering system used in this work was Emitech K675. It has three magnetron target assemblies with peltier cooling and a rotating sample table.

During sputtering process the chamber pressure is higher than in thermal evaporation and thus there can be more impurities in the deposited layer [97]. Because of the multiple collisions of the ions, the deposited material can come to the substrate from anywhere in the upper half-space. Thus the material is deposited also to the vertical parts of the substrate. For that reason only very thin layers can be deposited for lift-off process by sputtering, in this work mainly chromium adhesion layers for gold structures on fused silica substrates. In that case only 3 nm of chromium is needed.

4.1.2 Lift-off

In the last step of the lift-off process the actual lift-off is done. The substrate is placed in a solvent bath to dissolute the remaining resist and the metal on top of it. If the resist mask has a simple pattern like a two dimensional grating and it is high compared to the deposited metal thickness this step is usually quite easy. When more complex patterns and thicker deposited layers are introduced it can be more challenging to complete the process with no damages to the structure or redeposition of the removed material. For optical solutions such imperfections can be impairing.

When PMMA resist is used as a mask we can be sure that the

solvent, acetone dissolves all of the resist material but the metal on top of the resist forms small flakes floating in the solvent. If these flakes settle on the structure or on the substrate they are very hard or impossible to remove. This redeposition can be avoided by placing the substrate face down to the solvent bath and by changing the substrate to a clean solvent bath after most of the resist is removed, usually quite soon after placing the substrate in the first bath. To improve the solvent penetration to the smallest features the second bath can be placed to a ultrasonic washer. It can also be beneficial to heat the second bath in the ultrasonic washer to about 50 °C.

4.2 DRY ETCHING

Etching is a process in which material not covered with a mask is removed. Etching process using a liquid chemical etchant (typically some suitable acid) is called wet etching and a process with dry chemistry is called dry etching. Wet etching is an isotropic process which means that the material removal proceeds to all directions (with crystalline materials the etch rate can be different for different orientations of the crystal lattice). Dry etching is an anisotropic process meaning that the material removal is directional.

Dry etching uses free radicals or ions to remove material [73]. The ions and radicals are formed in plasma which is generated either in the same vacuum chamber with the substrate (reactive ion etching) or in a separate chamber from which they are directed to the substrate (ion beam etching) [62]. Plasma is generated by applying a radio frequency voltage between the two electrodes which makes free electrons oscillate and collide with gas molecules. Typical RF frequency is 13.56 MHz. One of the electrodes is inductively coupled to the RF generator. Since the other electrode is grounded, a dc bias voltage is developed between them. Former electrode becomes cathode and latter anode. Cathode gets negatively charged as electrons gather to it and inductive coupling to the RF generator prevents the charge from transferring over the capacitor. In etching process the substrate is placed on the cathode and the positive ions

of the plasma bombard it. If the energy of the ions is greater than 50 eV when hitting a surface, momentum transfer, bond breakage and lattice damage can occur to the etched material. The damaged atoms or molecules are very susceptible to attack by free radicals or ions [73].

Dry etching is typically a combination of physical and chemical processes, but can also be only one of them. Argon sputter etching and ion beam etching are purely physical processes. Reactive ion etching and reactive ion beam etching have both physical and chemical characteristics to make the process anisotropic. Purely chemical etching process is more isotropic so also the material under the mask is etched leading to rounded sidewalls in the structure [98].

4.2.1 Argon sputter etching

Argon sputter etching was tried the first time in the early 1960s for etching of semiconductor films, but it turned out unfeasible since the common photoresist masks degraded faster than silicon [73]. Being a purely physical process it requires the mask to be harder than the material to be etched to get at least as high structure to the substrate as the height of the mask. In figure 4.4 the typical process steps of argon sputter etching are presented. The patterning is done by EBL and mask by lift-off. The actual argon sputtering step is done in a reactive ion etching system, in our case in March CS-1701 from March Instruments. After sputter etching the mask is removed, if necessary for the usability of the structure. In this example process thermally evaporated titanium has been used as an adhesion layer in place of chromium so there wouldn't be any problems of structures detaching in mask removal step.

Positive argon ions from the plasma are extracted by the large field electric at the cathode and sputter that electrode at near-normal incidence [62]. The energy of the ions ranges from a few to several hundred electron volts, depending on the plasma conditions and chamber construction. Lowering the chamber pressure increases the energy of the ions as the bias voltage and mean free path of the

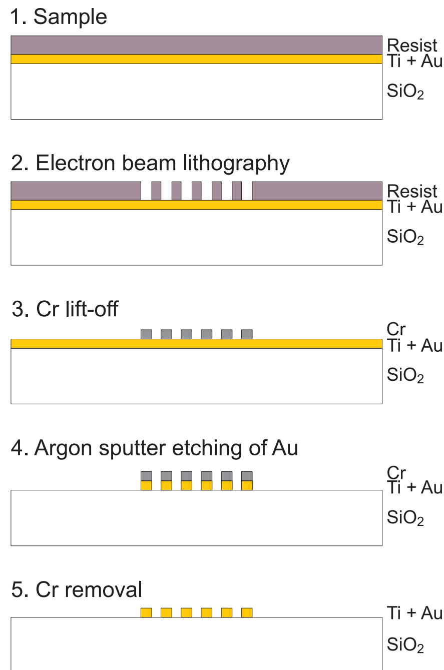

Figure 4.4: The steps of the argon sputter etching process.

ions increase. Etch rates are close to same for all materials but all in all they are slow, typically from ten to a few tens of nanometers per minute.

Besides being a slow process, argon sputter etching suffers also from bad profile of the etched structure. Usually sidewalls of the obtained structure are positively sloped. This results from the rounded corners of the mask [62]. The roundening of the mask corners is caused by the difference in etch rate with different incident angles. An ion hitting a surface in small angle needs less energy to remove material than an ion coming in larger angle. Also roughness in the walls of the structure can be harmful in optical solutions.

4.2.2 Reactive ion etching

Reactive ion etching (RIE) uses reactive chemical species to etch target material. Plasma is the source of the reactive species which

diffuse to the sample and form volatile products with the material to be removed [62]. Anisotropy is achieved by sidewall passivation; the etching process is tuned so that etch resistant material is being deposited to those parts of the structure which don't get ion bombardment, mainly sidewalls [99]. The sources of sidewall passivation material can be suitable precursors formed in plasma, erosion and redeposition of mask material or poorly volatile etch products of the material to be etched.

In the dry etching process both the material to be etched and the mask material are removed. The ratio of the these etching depths is called selectivity. Bigger selectivity leads to deeper etched structures with the same mask thickness. Therefore selectivity is a very important factor in the dry etching process.

All materials are naturally not reactive with the same process gases. Some materials are not reactive to any available gases and therefore the material range processable with reactive ion etching is limited. On the other hand, if the material is etchable and the selectivity is good, the etched structure can be a lot deeper with higher aspect ratio than structures made by lift-off.

RIE system can be equipped with a inductively coupled plasma (ICP) source. In ICP source the plasma is driven inductively with a power source operating also at 13.56 MHz [62]. ICP creates high-density, low-pressure, low-energy plasmas by coupling ion-producing electrons to the magnetic field arising from the RF voltage. For example for lithium niobate ($LiNbO_3$) the etch rate with ICP has been reported to be a lot higher than with only RIE [100]. Recently even gold, which has been thought to be a hard material for chemical dry etching, has been successfully etched with ICP [101].

The steps of a typical diffractive optical element fabrication process are shown in figure 4.5. The process starts with electron beam lithography and includes two reactive ion etching steps. Chromium is etched in chlorine-oxygen plasma and fused silica is etched in a gas combination of trifluoromethane (CHF_3), argon, and oxygen. Usually ZEP 7000-22 resist is used in EBL patterning since it has a good selectivity over chromium in chlorine based etching.

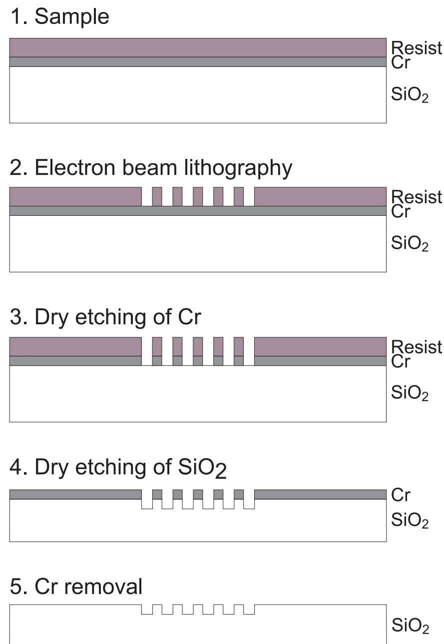

Figure 4.5: The steps of the fabrication of a diffractive optical element.

The two RIE systems used in this work were Plasmalab 100 with a ICP380 source and Plasmalab 80, both from Oxford Plasma technology. Plasmalab 80 system is smaller and used for oxide, nitride and silicon etching. Plasmalab 100 system uses also toxic gases (Cl_2, BCl_3 and HBr) and is therefore equipped with a vacuum loadlock for safe use. Besides etching of oxides, nitrides and silicon it can be used to etch chromium and aluminum. Both systems have helium back side cooling which improves thermal contact between the liquid cooled electrode and the substrate. By lowering the substrate temperature the durability of a resist mask can be improved.

Oxide and nitride etching

Oxides and nitrides are etched with fluorine-containing gases. Usually process gases are CHF_3, argon, and oxygen. Other fluorine-containing gases which can be used in oxide and nitride etching

are CF_4 and SF_6. Adding of oxygen increases fluorine to carbon ratio which increases etch rate [62]. On the other hand, oxygen attacks heavily to polymers so it reduces selectivity when a resist mask is used. Therefore a metal mask is preferred in oxide and nitride etching. Selectivity of silicon dioxide to chromium is usually from 30 to 36 in our common etching process while to PMMA it's less than one and to ZEP from 1 to 2. In this work chromium was used as a mask material in the etching of silicon dioxide (SiO_2) and silicon nitride (Si_3N_4).

Chromium etching

Chromium etching is done in chlorine atmosphere. By adding a suitable amount of oxygen the etch rate of chromium can be increased without losing the selectivity over the resist mask [102]. Helium back side cooling has also been found to improve etching result.

Chromium etching can be done using a durable resist, such as ZEP or HSQ, or some oxide, such as silicon oxide (SiO_2) or titanium oxide (TiO_2), as a mask. When using hard mask one has to ensure that the mask is pore-free and uniform. To achieve this the mask has to either evaporated in good vacuum or deposited by ALD. Selectivity of chromium to ZEP is from 1 to 1.5 which is in most cases good enough.

Aluminum etching

Chlorine based techniques are used also for aluminum etching, but to that process boron trichloride (BCl_3) needs to be added to get through the native oxide layer on top of aluminum. Oxides have a very high etch resistance to chlorine plasma and therefore they can be used as durable masks in chromium and aluminum etchings. Only the deposition of pore-free oxide on top of the metal layer can be troublesome. Pores and ununiformities in the oxide mask cause holes and surface roughness to the etched metal structure.

Also the quality of the aluminum layer affects the outcome of the etching process. In figure 4.6 two dry etched aluminum grids are shown. Both structures are etched with a ZEP resist mask and the remained mask material has been removed by oxygen plasma before imaging. The structure in figure 4.6(a) is etched to a 400 nm thick aluminum film deposited in our department. The film was thermally evaporated in low vacuum. After this test the quality of our own aluminum layers has been improved by lowering the chamber pressure with titanium evaporation before the aluminum evaporation. This way the chamber pressure can be lowered to about 2×10^{-7}. The structure in figure 4.6(b) is etched to a commercial 400 nm thick sputtered aluminum film from Nanofilm, Inc. In both cases exactly the same etching process has been used, but the quality of the etched structure is totally different. With our own aluminum the etching process hasn't gotten through the layer, but the structure under the mask has already gotten heavy damage. With commercial aluminum the etching process has gone through the layer and no undercutting is seen. Still some pores, shape variations and distinguishable material defects are seen also in figure 4.6(b). Therefore the first step in fabrication of aluminum micro- and nanostructures is to get good quality aluminum films.

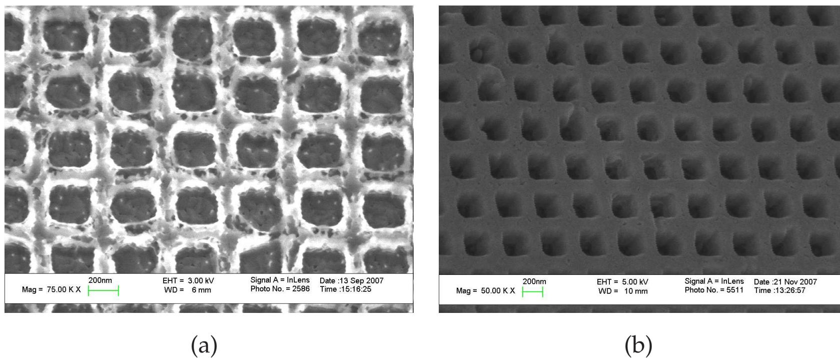

(a) (b)

Figure 4.6: Inductive grids made by dry etching to thermally evaporated aluminum deposited in our department (a) and commercial sputtered aluminum (b).

Silicon etching

Silicon etching can be done both in RIE and in ICP systems. In RIE the etching is fluorine based (process gases are usually either CHF_3 or SF_6 and oxygen). The etch rate is slow but sufficient for shallow structures like molds for nanoimprint lithography [35]. RIE etching of silicon can suffer from isotropy. In figure 4.7 cut profile and tilt view of a square hole array etched to silicon by RIE is presented. Using ICP and a gas combination of hydrogen bromide (HBr) and oxygen the etching speed can be increased and anisotropy enhanced [103]. Cl_2 based ICP processes are also used but HBr gives better structure shape [104].

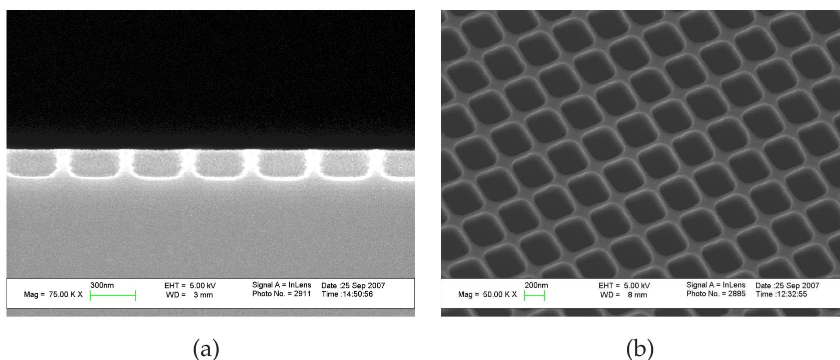

(a) (b)

Figure 4.7: RIE etched hole array in silicon from side (a) and tilt (b) views.

4.2.3 Reactive ion beam etching

Reactive ion beam etching (RIBE) system combines the physical and chemical etching processes effectively. Material is removed by processes that are mainly physical and therefore metal masks are preferred over resist masks. Also the quality of the mask has a bit bigger role in the outcome of the etching than in reactive ion etching.

The reactive ions are generated in a separate ion source and driven to the substrate with applied voltage. One big advantage of this system is that the sample can be rotated to change the incident

angle of the ions. This allows fabrication of overhanging structures like slanted gratings (see figure 4.8). Such gratings can be used as light couplers [105, 106]. Reactive ion beam etching has been used to etch for example SiO_2 [107, 108] and $LiNbO_3$ [109]. The RIBE system used in this work was Ionfab 300 Plus from Oxford Plasma technology.

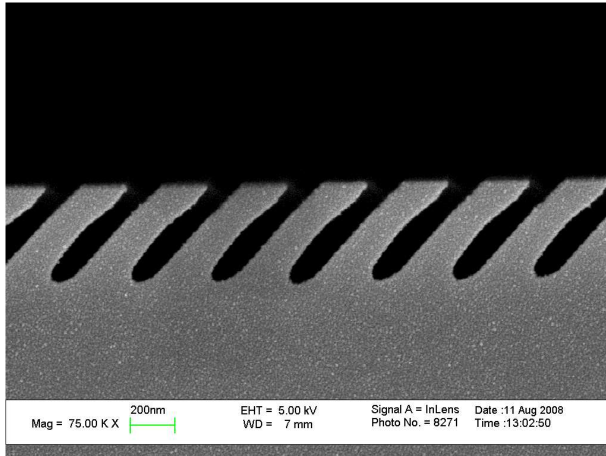

Figure 4.8: Cut profile of a slanted grating in quartz made by reactive ion beam etching.

4.2.4 Effect of mask quality

Mask shape and hardness affect the outcome of the dry etching process. Resist masks are easy and straightforward to make and use, but they are also soft compared to metal masks. If the etching process is long, soft mask can start to rounden from corners and it results in positive sloped profile in the etched structure. One has to remember also that differences between resist materials are big. PMMA is not a good mask for dry etching because of its softness and poor etch resistance. On the other hand ZEP and HSQ resist can be very durable in dry etching, especially when the etching is done in chlorine atmosphere.

Chromium mask can be done by lift-off, wet etching or dry etching. Wet etching is not a good option for micro- and nanostructures

since it is an anisotropic process and therefore leads to heavy undercutting, but for larger structures it works fine. As an example of the effect of mask quality, in figure 4.9 reactive ion beam etched structures in fused silica are shown. In both cases the chromium mask was made by lift-off and it was 50 nm thick. In 4.9(a) the substrate was rotated during the chromium evaporation and in 4.9(b) the substrate was placed straight above the source. Same masks were shown earlier in figure 4.3. Since the mask made with rotation is thinner from the edges it degrades faster, which results in more triangular profile of the slanted grating.

Dry etched chromium masks are more rectangular than masks made by lift-off as can be seen in figure 4.10(a). Therefore also the structure profile of the reactive ion beam etched fused silica is better compared to those gotten with lift-off masks (Fig. 4.10(b)). The thickness of the chromium mask was also in this case 50 nm and the reactive ion beam etching was done in the same run with lift-off samples. Even though the source material is the same as in lift-off masks there is less mask erosion during etching. Therefore dry etched mask has lasted the whole 20 minutes 50 seconds long etching process since the top part of the structure is smooth where as in structures in figure 4.9 the top part is rough. The structure in

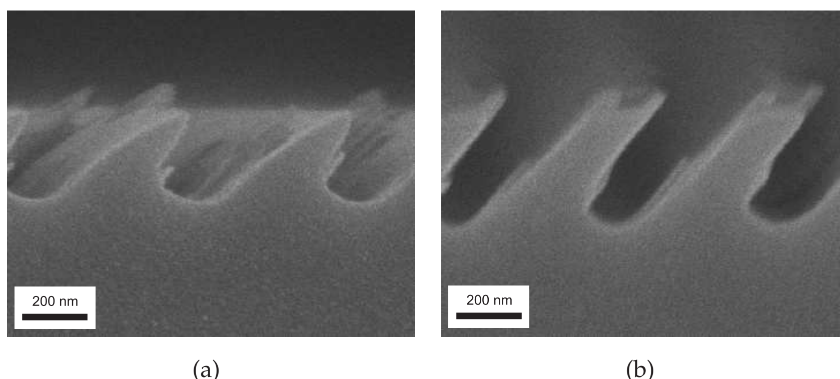

(a) (b)

Figure 4.9: Reactive ion beam etched structures in fused silica. In (a) the chromium mask was made by lift-off with the substrate rotating during evaporation and in (b) the sample was placed straight above the source.

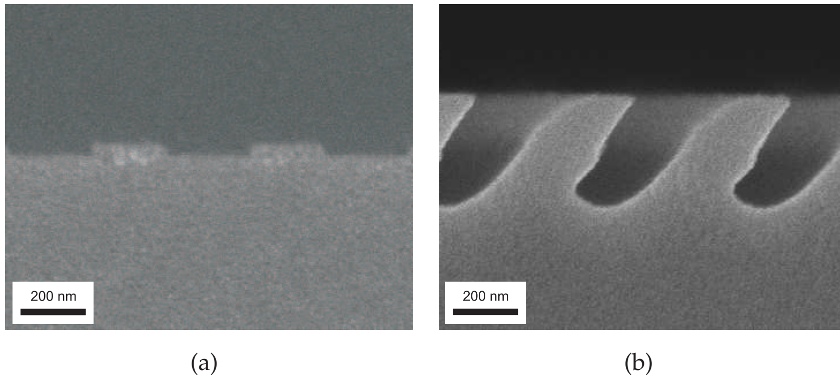

Figure 4.10: Dry etched chromium mask (a) and reactive ion beam etched structure in fused silica (b).

figure 4.10(b) is all in all quite smooth although the profile is not optimal.

4.3 ELECTROCHEMICAL DEPOSITION

Electroplating and electroforming are forms of electrochemical deposition with slightly different goals. Both are used among other processes in the fabrication of micro- and nanostructures and are thus discussed in this section. Electrochemical deposition, or electrodeposition, involves ion diffusion and migration in an electric field, and the reduction of the charged growth species at the growth or deposition surface [110]. The target to be plated needs to be either conductive itself or it has to have a conductive seed layer on top of it. For optical solutions this seed layer can destroy the usability of the element, because it's not fully transparent and therefore it should be removed before the use of the structure.

Electroplating in general refers to a process where the aim is to cover conductive surfaces with thin films for example for corrosion protection [111]. The thickness of the electroplated layer can be controlled with the plating time. By introducing a mask on top of the seed layer or conductive substrate one can make the electrochemically deposited material to grow only to the mask openings.

One way of masking the substrate is to use a resist mask patterned by electron beam lithography (Fig. 4.11). The fabrication process starts with EBL and the grooves of the developed resist are then filled with metal by electrochemical deposition starting from the seed layer under the resist mask. For example this method has been used to create X-ray optics [112].

Electroforming refers to a process where the goal is to replicate the pattern from a master to metal. Probably the most known microfabrication process exploiting electroforming method is the LIGA (acronym from german words Lithographie, Galvanoformung and Abformung, i.e. lithography, electroplating and molding) process [113]. In LIGA patterning is done by optical lithography but similar process can be done using any patterning method. In figure 4.12 the steps of a typical nickel mold process are presented. Again the patterning is done by electron beam lithography. In this case the resist structure (could be also for example dry etched fused silica or silicon) and the substrate is covered with a thin evaporated or sputtered metal seed layer. Electrochemical deposition is then used

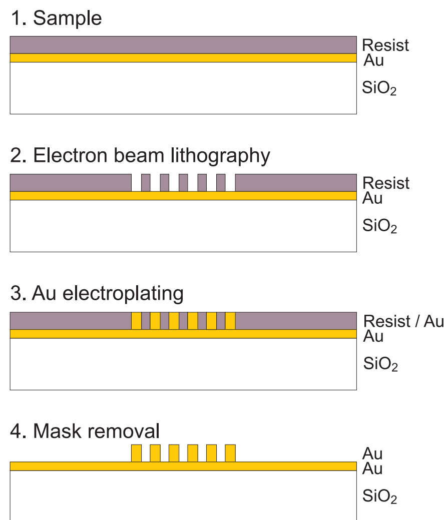

Figure 4.11: The steps of the fabrication process for micro- and nanostructures by electroplating.

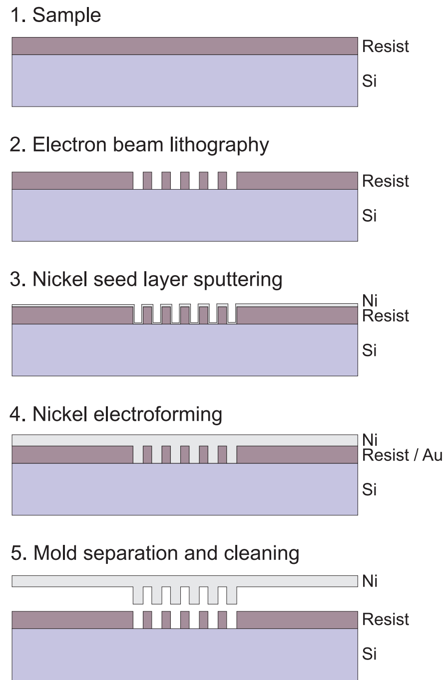

Figure 4.12: The steps of the fabrication process for a nickel shim with micro- and nanostructures by electroforming.

to bury the master structure and to form a durable plate under the replicated structure. In the separation step some resist is left in the metal replica and it can be removed with a proper solvent. In figure 4.13 a nickel plate and SEM image of the structure in it are shown.

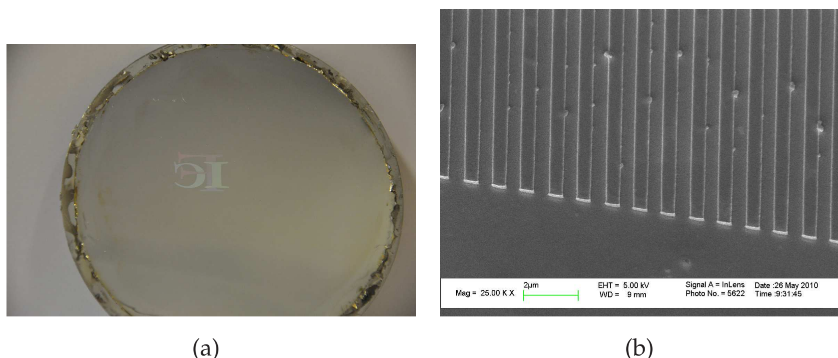

(a) (b)

Figure 4.13: Nickel plate made by electroforming (a) and SEM image of the structure in it (b).

4.4 ATOMIC LAYER DEPOSITION

Atomic layer deposition (ALD) is a coating technique where the material is grown in a cyclic manner [114]. In the simplest case, one cycle consist of four steps: (1) exposure of the first precursor, (2) purge or evacuation of the reaction chamber, (3) exposure of the second precursor, and (4) purge or evacuation [115]. Molecules of the first precursor either react with functional groups on the surface or chemisorb. Only a monomolecular layer of precursor can attach to the surface and the following purge or evacuation removes the rest of the material. The second precursor reacts with the monolayer forming the desired solid. The number of cycles determines the thickness of the deposited layer as each cycle increases the deposited thickness with exactly the same amount.

Compared to evaporation and sputtering techniques the material distribution is totally different in ALD. No geometrical limitations exist as long as process gases can get to the surface. Therefore the same amount of material is deposited to every open surface forming a good quality and uniformity thin film. If the number of cycles is set high enough the original structure can be buried in the same way as in electroforming.

One restriction of the applicability of the method is the temperature of the reactor in which the deposition takes place and recently

a lot of research has been going on to lower it [116]. So far in most cases the reactor temperature is so high that organic materials can't be coated without damaging them. Another drawback is the slowness of the process, but in research it doesn't usually matter and for mass production the batch size can be increased. ALD process can be used to deposit oxides, nitrides and metals [114]. The process has been used to fine-tune surface properties [96] and to reduce the feature size of slot waveguides [117]. The iridium deposition done by ALD presented in the chapter 5 has been performed at the Department of Chemistry in the University of Helsinki.

5 Applications for metallic micro- and nanostructures

In this chapter some of the applications, for which elements have been fabricated by the author using the techniques described in chapter 4, are presented. Based on the electromagnetic theory described in chapter 2 the optical properties of the fabricated structures are briefly discussed. The optical response of the structures has been simulated using a numerical method based on the rigorous diffraction theory, the Fourier modal method, because analytical functions are known only for a very limited number of geometries [118].

5.1 SECOND HARMONIC GENERATION

As already discussed in section 2.2.2 metal structures can give rise to nonlinear optical effects if they are correctly designed. Second harmonic generation (SHG) is one of the most studied nonlinear effects. Previously the effects exhibiting the highest enhancements have depended mainly on the intensity of the local field. However, fundamental phase and symmetry considerations dictate that second-order nonlinear optical processes (such as SHG) require noncentrosymmetry [44]. Strong fields alone may then be insufficient for SHG if the sample is centrosymmetric.

To study SHG experimentally we have fabricated T-shaped gold structures with variable gap size between horizontal and vertical bars on a fused silica substrate by lift-off process (see figure 5.1). The bar length of the structure was 250 nm and width 125 nm. Period of the structure was 500 nm in both directions. 5 nm thick sputtered chromium adhesion layer was used under the 20 nm thick evaporated gold layer. Finally a 20 nm thick fused silica layer was evaporated to protect the structures from detaching in high power

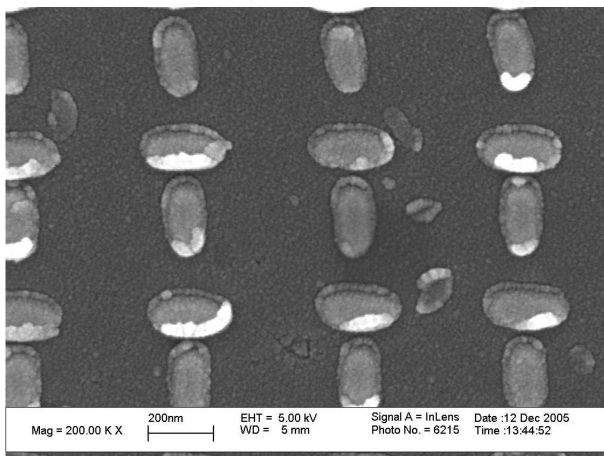

Figure 5.1: T-shaped gold structures on a fused silica substrate made by lift-off process.

laser measurements.

It was shown that the SHG response is driven by localized enhancement of the nearly resonant fundamental field [26, 27]. The strongest fundamental fields occur at the particle boundaries (see Fig. 5.2), which means that the SHG responses arise through the local surface susceptibility of the metal particles. The SHG responses depend on the size of the gap between the horizontal and vertical bars, but they don't decrease linearly as one could deduce from theory [119]. The largest gap (40 nm) gives weak SHG responses for both components, as might be expected from theory which predicts that the gap must be small (a few nanometers or less) to enhance the SHG response [119,120] and from experimental evidence of overlapping cylindrical apertures [121].

The SHG response of noncentrosymmetric T-shaped gold structures with gaps is dominated by the polarization and symmetry of the distribution of local fields in the structure [28]. Strong local fields in the gap are not alone sufficient for efficient SHG, because of the noncentrosymmetry requirement of second-order processes. Also the local-field distribution and its polarization properties can exhibit a sensitive and complicated dependence on the gap size.

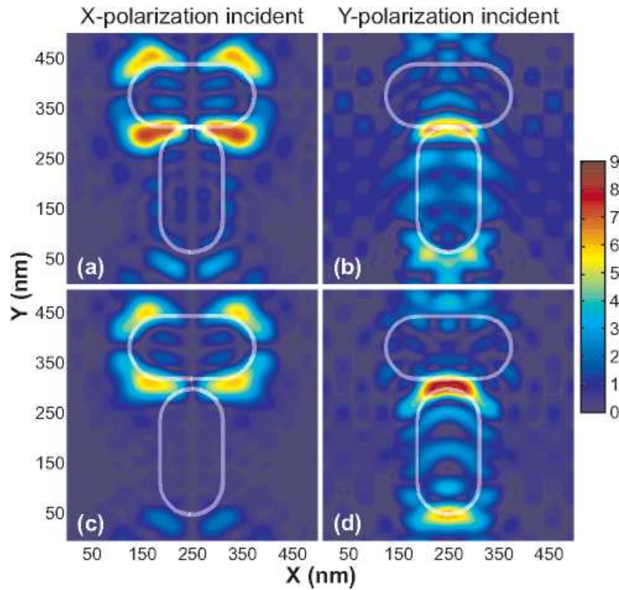

Figure 5.2: Electric field Y-component distributions for incident X and Y-polarizations, as indicated by the column headings: (a,b) 1 nm nanogap; (c, d) 20 nm nanogap [26].

The local fields can contain strong polarization components which do not exist in the incident field. They arise from the low structural symmetry and drive the nonlinearity efficiently. Therefore the tensorial properties of the strong nonlinear signals depend in a nontrivial way on the gap size and the overall symmetry of the structure. It is possible that a relatively large gap gives rise to a particular component of the measured strong nonlinearity.

It has also been shown that SHG from T-shaped gold nanostructures is significantly influenced by the chiral symmetry breaking that arises from the nonorthogonal mutual orientations of its horizontal and vertical bars. In particular, the responses of left- and right-hand circularly polarized (LCP and RCP, respectively) light differ. Circular-difference response (CDR) can be calculated from the second harmonic intensities for LCP and RCP using [122]

$$CDR = \left| \frac{I_{LCP} - I_{RCP}}{(I_{LCP} + I_{RCP})/2} \right|. \tag{5.1}$$

Because the individual bars are symmetric, the effect must arise from their mutual coupling. It would be expected that the smallest gap should lead to the strongest coupling and thus the highest chiral signatures. Contrarily it was found that the chiral signatures for the smallest gaps were weak and that they peak for a larger gap size (see Fig. 5.3). This is caused by the polarization-dependent local field distribution of the fundamental light in the structure for LCP and RCP. [29]

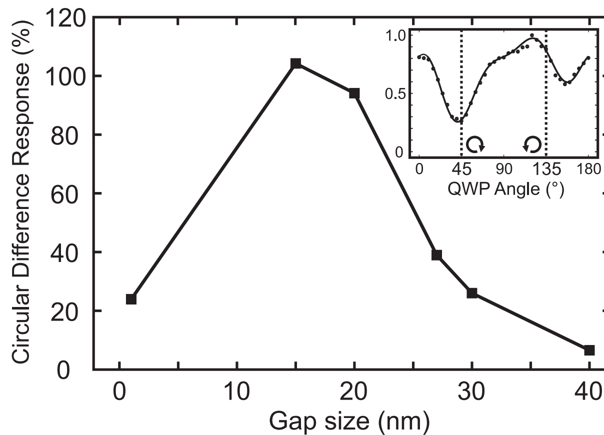

Figure 5.3: Circular-difference response as a function of gap size. Inset: Normalized SHG intensity from a sample with a 15 nm gap as a function of the quarter wave plate angle. The solid curve is a fit to a theoretical model. Vertical dashed lines indicate the circular polarization states. [29]

5.2 ENHANCED OR SUPPRESSED TRANSMISSION

Inductive grids (Fig. 4.6 in page 37) can be designed to have either enhanced or suppressed transmission [30, 31]. Inductive grid filters are used to block electromagnetic radiation after some cut-off wavelength. They are widely used in the mirrors of radio telescopes and in the doors of common microwave ovens.

We aimed to develop a method to produce filters that are able to reject near-infrared radiation but transmit shorter wavelengths [30]. To reject radiation with wavelength above 1 μm the period of the

grid should be less than 400 nm [48]. The thickness of the grid affects the absorption of infrared radiation, while the effective area of the holes of the grid is responsible for the transmission in the short wavelength region. To fulfill both requirements one should be able to produce narrow metal lines with high aspect ratio. To avoid unwanted losses of X-ray radiation, the filters should be free-standing. The fabrication process started with patterning by electron beam lithography. The pattern was transferred from resist to evaporated fused silica layer on a silicon substrate by dry etching. Then the grooves in fused silica were filled with iridium by ALD and the excess iridium on top of the mask was removed by argon sputter etching. Finally the structure was made free-standing by removing the substrate from under the grid by wet etching of silicon. The fabricated free-standing iridium grid is shown in figure 5.4(a) from front side and in figure 5.4(b) from back side. Period of the structure was 400 nm, line width 80 nm and thickness 400 nm. Calculated and measured transmittance of the grid is shown in figure 5.5. Experimental transmittance is a bit lower than predicted by calculations in the visible region. It is most likely caused by the particles on top of the grid (see Fig. 5.4(a)). These particles are suspected to be unremovable residual of the polyimide coating used to protect the structure during the through wafer etching.

We have also studied the extraordinary transmission of induc-

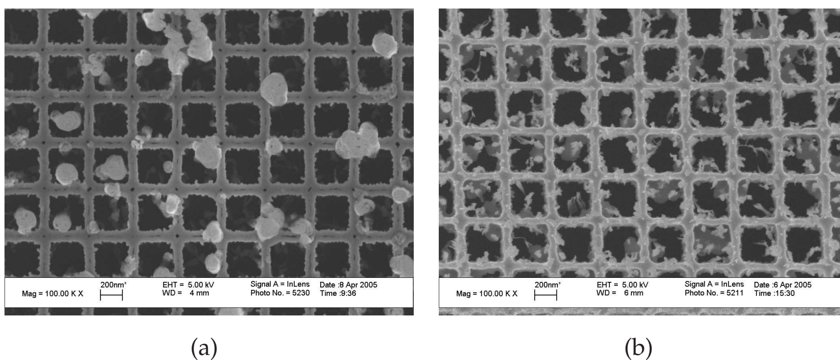

Figure 5.4: Inductive grid filter made of iridium from front (a) and back (b) sides [30].

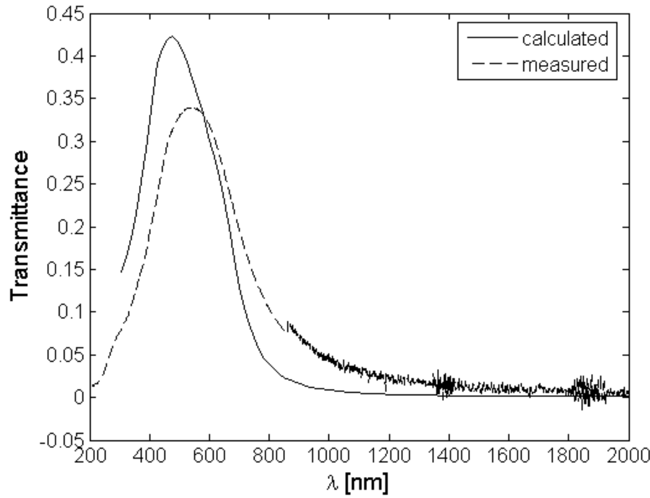

Figure 5.5: Calculated and measured transmittance of the inductive grid filter made of iridium [30].

tive grids [31]. The effect is mediated by surface plasmons in periodically perforated metal films and it has been well known for many years [123]. There has been a lot of discussion whether the role of surface plasmons is positive or negative [42, 124–127], it has been commonly admitted that the transmission effect involves two major contributions: the resonant excitation of surface plasmon polaritons (SPPs) on the continuous metal surface and the nonresonant excitation of cavity surface plasmons (CSPs) localized in the holes [127–130]. The diffraction modes of the grating can be coupled to both the SPPs and CSPs; it is the interference between the resonant and nonresonant processes that leads to the Fano-type profile of the transmission spectrum [128, 129].

To study this effect we have fabricated a gold inductive grid on a fused silica substrate by electron beam lithography and lift-off. The period of the grid was 800 nm, hole size 375 nm and thickness 65 nm. A 3 nm chromium adhesion layer was sputtered on the sample before gold evaporation. The fabricated structure is shown in figure 5.6(b). Its transmittance and reflectance were measured at various

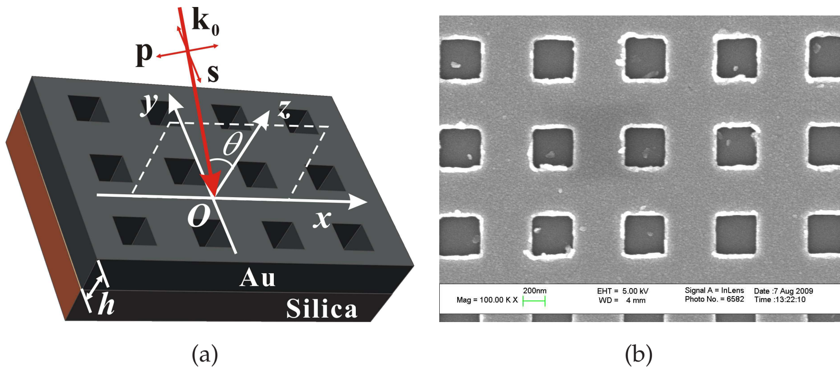

Figure 5.6: Geometry of the inductive grid measurements (a) and fabricated gold grid on a fused silica substrate (b) [31].

incident angles by spectroscopic ellipsometry (with a variable angle spectroscopic ellipsometer VASE from J. A. Woollam Co.) in the wavelength range 1000 $\sim$ 1600 nm for both p- and s-polarization. Geometry and notations of the setup are shown in figure 5.6(a). The results of the transmittance measurements are shown in figure 5.7.

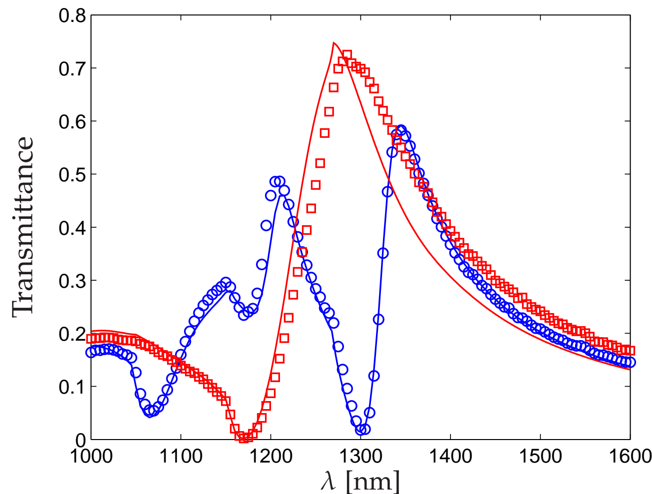

Figure 5.7: Calculated and measured transmittance of the inductive grid made of gold. Blue circles and lines are measured and calculated values for p-polarization and red squares and lines are measured and calculated values for s-polarization, respectively.

Comparing the two polarization cases (p and s), we can see that the polarization-dependent transmission behavior arises from the lift of degeneracy of the SPP modes at oblique incidence. For s-polarization, in the interested spectral range, only the $(0, \pm 1)_{\text{sub}}$ SPP modes on the gold-silica interface are excited (consistent with the TM-excitation condition of SPPs in Ref. [42]), whose dispersion is still degenerate due to the symmetry of the two modes with respect to the incidence plane and exhibits small dependence on the incident angle θ. For p-polarization, however, the $(\pm 1, 0)_{\text{sub}}$ SPP modes are excited in the gold-substrate interface (denoted with sub), whose dispersion is further split due to the asymmetrical excitation condition of the two modes in the incidence plane and is therefore very sensitive to θ. Consequently, as the transmittance of s-polarized case remains almost unchanged with respect to the normal incidence case with the increase of θ in the Oxz plane, the transmission peak of the p-polarized case turns drastically to a dip. By adjusting the splitting of SPP dispersion by incident angle θ, we can thereby achieve the polarization-switching enhanced/suppressed transmission at a given wavelength $\lambda = 1300$ nm. Transmittance of the structure predicted by geometrical optics is about 0.22. For our structure the transmittance of s-polarized light was about 0.7 so the enhancement factor is about 3.2.

5.3 POLARIZATION ROTATION

Besides having a suppressed or enhanced transmission, an inductive grid can have also simultaneously optical activity [32]. With our gold film with chiral holes (fig. 5.8) we were able to rotate the polarization of incoming light. The structure was made by electron beam lithography and lift-off process. Compared to the previously studied chiral structures [131–135] our structure is complementary which enables enhanced transmission. The optical property of the structure was characterized with spectroscopic ellipsometry. In figure 5.9 calculated and measures transmittance and polarization rotation of the structure as well as ellipticity of the transmitted light

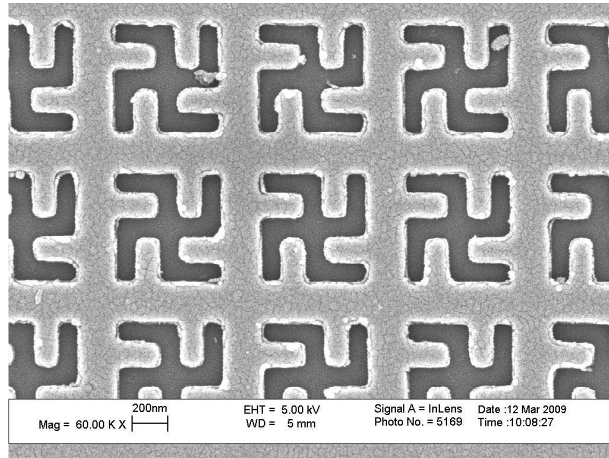

Figure 5.8: Gold grid with chiral holes on a fused silica substrate.

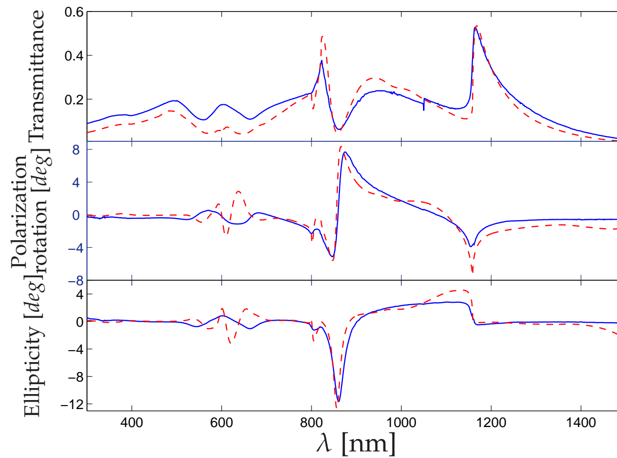

Figure 5.9: Calculated and measured transmittance of the inductive grid with chiral holes made of gold. Blue solid lines present measured values and red dashed lines calculated values [32].

beam are shown.

The principle and optical performance of the proposed structure was demonstrated. An enhanced transmittance peak of 53% was observed at wavelength 1168 nm accompanied nearby by a po-

larization rotation peak (about 8° in theory and 4° in experiment) at normal incidence. The effective specific rotatory power reaches 10^5 deg/mm, which is one or two orders of magnitude larger than that of previous particle-type 2D metallic planar chiral structures and several orders larger than that of natural chiral media. When the thickness is 50 nm or higher it has only a slight effect on the transmittance. Below the thickness of 50 nm the transmittance gets lower when thickness is increased.

5.4 ASYMMETRICAL EXCITATION OF SURFACE PLASMON POLARITONS

In the earlier studies the optical excitation of surface plasmon polaritons has been done by prism coupling, with topological defect on the surface or with periodic corrugation in the surface [136]. To control the direction of the propagating surface plasmon, oblique angle of incidence has been used [137,138], but for simplicity of the optical set up it would sometimes be better to be able to work with normal incidence.

Kleemann *et al.* have introduced a two dimensional binary grating, called the blazed area-coded effective-medium structure (BLACES), in which the index distribution of the element can be quite easily tailored [139]. The gradient local effective dielectric constant of the grating layer for x-polarized incidence can be calculated from [140]

$$\epsilon_{\text{eff}}(x) = \epsilon_{\text{met}} f(x) + \epsilon_{\text{die}}[1 - f(x)], \tag{5.2}$$

where $f(x)$ is the local fill factor of metal at a given x. We implemented the same idea to unidirectional coupling of surface plasmon polaritons excited with light coming in normal incidence [33]. When the grating is mounted under normal incidence and the SPP is to be excited by the $\pm$1st orders, momentum conservation can be satisfied by

$$\boldsymbol{k}_{\text{SPP}} = \pm K\hat{\boldsymbol{x}}. \tag{5.3}$$

The fabrication process included electron beam lithography and lift-off. The resulting gold layer with triangular holes is presented in

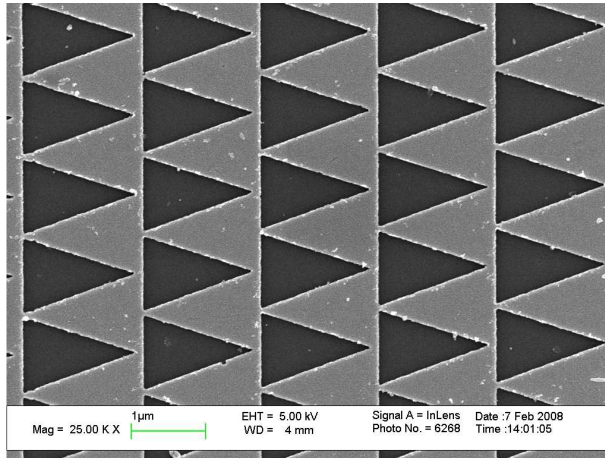

Figure 5.10: Gold layer with triangular holes for asymmetrical coupling of surface plasmon polaritons [33].

figure 5.10.

A scanning near-field optical microscope (SNOM) was used to characterize the surface plasmon coupling [33]. In figure 5.11 the near-field strength, i.e. square root of the field intensity, scanned across the illumination spot is presented. The scan length was 100 μm and the wavelength was changed from 1460 to 1580 nm with a step of 4 nm. The spot diameter was about 20 μm. We can con-

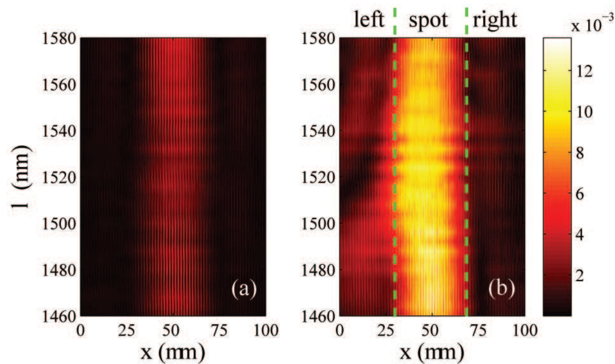

Figure 5.11: Near-field strength scanned in x direction across the illumination spot for TE (a) incidence and TM (b) incidence. The amplitude scale is in arbitrary units. [33]

clude that though the asymmetrical coupling effect was weak, it corresponds well with the simulations.

5.5 MASS FABRICATION

Since the use of micro- and nanostructures is all the time increasing in consumer goods, there is also a need for mass fabrication of them. The fabrication of the original surface structure can cost a lot, but it doesn't matter if there is a cost effective way to replicate the structure. If the costs of the original structure can be divided between thousands of replicated pieces, the cost per unit can become acceptable. The copying of surface-relief micro- and nanostructures can be done by replication techniques such as hot embossing [141–143], (micro) injection molding [141, 144, 145], or UV-moulding [141, 146, 147]. In figure 5.12 roll-to-roll replicated beam shaping lenses from Nanocomp Oy Ltd and the system they are made with are shown. These very thin (less than 0.385 mm) and flexible lenses are used in LED light collimation.

Electroforming is one way of fabricating a stamp for replication.

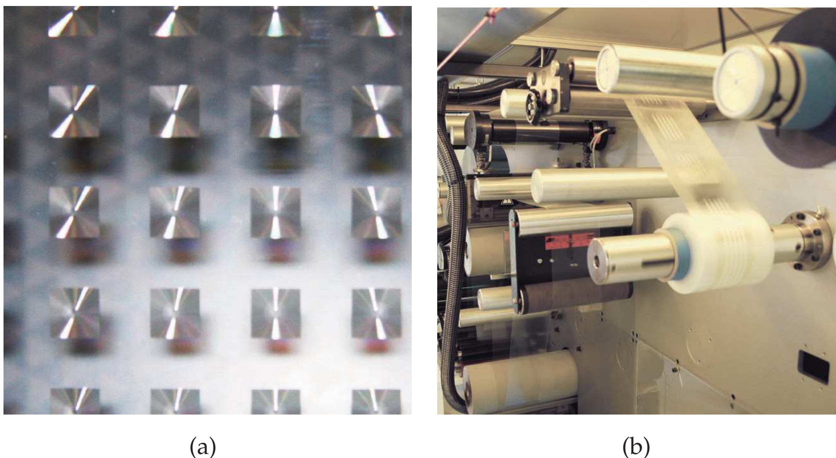

(a) (b)

Figure 5.12: Roll-to-roll replicated NAFLENS beam shaping lenses (a) and roll-to-roll replication system (b). The lenses are used LED light collimation. Images courtesy of Nanocomp Oy Ltd.

It has been used to replicate for example dielectric diffractive optical elements [148]. The master structure can be made by electron beam lithography and dry etching. By introducing an intermediate UV-moulding step the original master structure can be saved [34]. UV-moulding can be used to replicate structures even with very sharp features [149] and it doesn't do any damage to the original master structure. Therefore it can be repeated many times if necessary. The metal stamp used in replication will inevitably get damaged in use and it has to be replaced. If the original master is still usable the fabrication costs of a new master will be saved.

Mass fabrication of metallic micro- and nanostructures is not as simple as of dielectrics. There are no one-step processes for replicating metal structures. One possibility could be to use roll-to-roll nanoimprint lithography [150] to make masks for further processing. Replicas with masks could be then used in lift-off or etching processes in large batches.

6 Conclusions

Methods for fabricating metallic micro- and nanostructures have been discussed. The desired material and structure depth limit the choice of fabrication method. If more than one possible method exists, thought should be given to the effect of the chosen method to the shape of the final structure. The simplest available method might lead to undesired features in the structure.

Some applications of the metal structures and their theoretical background were presented. The applications include structures for experimental basic research as well as application directed filtering devices and mass fabrication. Most of the structures were made by lift-off which is a simple method for creating shallow structures, but doesn't work that well for high aspect ratio structures. For those cases dry etching, electrochemical deposition and ALD methods were considered.

The controllable fabrication of metallic micro- and nanostructures is a demanding task. Electron beam lithography is a flexible though slow method for pattering of micro- and nanostructures. Slowness is not a problem in research environment where high throughput is not needed. Fortunately, for mass fabrication there are multiple ways of replicating the original master structure which makes the use of microstructures feasible also in consumer products. For metallic structures mass fabrication is not as simple as for dielectric structures, but new methods will be developed to overcome the problems in it.

Although some applications of metallic micro- and nanostructures, like surface enhanced Raman scattering (SERS) [14] used in spectroscopy, are already at mature commercial stage, there is still plenty of room for basic research. When using correct fabrication methods and materials the promising optical effects of the metal structures can be realized. Before proceeding to fabrication the optical response of the structure should be carefully simulated.

Improved computational power and more accurate modeling algorithms help to come up with new designs possibly with more complex features. When modeling can be done reliably the risk of wasting time in the fabrication can be lowered and the desired optical effects realized. To get accurate simulations it is better to use complex refractive index measured from a similarly deposited metal film, because the refractive index of a deposited thin film differs from values measured from bulk material. Also the limitations of the fabrication processes, e.g. the maximum thickness of the structure and the roundening of its corners, should be considered and taken into account in the simulation.

Many research groups in the world have concentrated on metallic micro- and nanostructures. There is proof of their potential, not just for basic research but also for commercial use. Plasmonic structures can be used for example in biosensing [11] which is nowadays one of the hottest research topics in photonics. Also the use in optical switching [151] and computing [2] could happen in future in a large scale. A lot of work has to be done to realize the potential of metallic nanostructures, but it is in any case very probable that we will benefit from them more and more in the future.

References

[1] S. A. Maier and H. A. Atwater, "Plasmonics: Localization and guiding of electromagnetic energy in metal/dielectric structures," *Journal of Applied Physics* **98,** 011101 (2005).

[2] E. Ozbay, "Plasmonics: Merging Photonics and Electronics at Nanoscale Dimensions," *Science* **311,** 189–193 (2006).

[3] R. Zia, J. A. Schuller, A. Chandran, and M. L. Brongersma, "Plasmonics: the next chip-scale technology," *Materials Today* **9,** 20–27 (2006).

[4] J. B. Pendry, "Negative Refraction Makes a Perfect Lens," *Physical Review Letters* **85,** 3966–3969 (2000).

[5] R. A. Shelby, D. R. Smith, and S. Schultz, "Experimental Verification of a Negative Index of Refraction," *Science* **292,** 77–79 (2001).

[6] D. R. Smith, J. B. Pendry, and M. C. K. Wiltshire, "Metamaterials and Negative Refractive Index," *Science* **305,** 788–792 (2004).

[7] V. M. Shalaev, W. Cai, U. K. Chettiar, H.-K. Yuan, A. K. Sarychev, V. P. Drachev, and A. V. Kildishev, "Negative index of refraction in optical metamaterials," *Optics Letters* **30,** 3356–3358 (2005).

[8] D. R. Smith, S. Schultz, P. Markoš, and C. M. Soukoulis, "Determination of effective permittivity and permeability of metamaterials from reflection and transmission coefficients," *Physical Review B* **65,** 195104 (2002).

[9] D. Schurig, J. J. Mock, B. J. Justice, S. A. Cummer, J. B. Pendry, A. F. Starr, and D. R. Smith, "Metamaterial Electromagnetic Cloak at Microwave Frequencies," *Science* **314,** 977–980 (2006).

[10] A. Sihvola, "Metamaterials in electromagnetics," *Metamaterials* **1,** 2–11 (2007).

[11] J. N. Anker, W. P. Hall, O. Lyandres, N. C. Shah, J. Zhao, and R. P. Van Duyne, "Biosensing with plasmonic nanosensors," *Nature Materials* **7,** 442–453 (2008).

[12] M. E. Stewart, C. R. Anderton, L. B. Thompson, J. Maria, S. K. Gray, J. A. Rogers, and R. G. Nuzzo, "Nanostructured Plasmonic Sensors," *Chemical Reviews* **108,** 494–521 (2008).

[13] A. Otto, I. Mrozek, H. Grabhorn, and W. Akemann, "Surface-enhanced Raman scattering," *Journal of Physics: Condensed Matter* **4,** 1143 (1992).

[14] A. Campion and P. Kambhampati, "Surface-enhanced Raman scattering," *Chemical Society Reviews* **27,** 241–250 (1998).

[15] P. L. Stiles, J. A. Dieringer, N. C. Shah, and R. P. Van Duyne, "Surface-Enhanced Raman Spectroscopy," *Annual Review of Analytical Chemistry* **1,** 601–626 (2008).

[16] A. Tredicucci, C. Gmachl, C. Gmachi, F. Capasso, A. L. Hutchinson, D. L. Sivco, and A. Y. Cho, "Single-mode surface-plasmon laser.," *Applied Physics Letters* **76,** 2164 (2000).

[17] V. J. Sorger, T. Zentgraf, R.-M. Ma, C. Gladden, L. Dai, G. Bartal, and X. Zhang, "Plasmon lasers at deep subwavelength scale," *Nature* **461,** 629–632 (2009).

[18] M. Brust, M. Walker, D. Bethell, D. J. Schiffrin, and R. Whyman, "Synthesis of Thiol-derivatised Gold Nanoparticles in a Two-phase Liquid-Liquid System," *Journal of the Chemical Society, Chemical Communications* 801–802 (1994).

[19] Y.-Y. Yu, S.-S. Chang, C.-L. Lee, and C. R. C. Wang, "Gold Nanorods: Electrochemical Synthesis and Optical Properties," *The Journal of Physical Chemistry B* **101,** 6661–6664 (1997).

[20] G. Schmid, M. Bäumle, and N. Beyer, "Ordered Two-Dimensional Monolayers of Au_{55} Clusters," *Angewandte Chemie International Edition* **39,** 181–183 (2000).

[21] Y. Maeda, H. Tabata, and T. Kawai, "Two-dimensional assembly of gold nanoparticles with a DNA network template," *Applied Physics Letters* **79,** 1181 (2001).

[22] M. M. Maye, S. C. Chun, L. Han, D. Rabinovich, and C.-J. Zhong, "Novel Spherical Assembly of Gold Nanoparticles Mediated by a Tetradentate Thioether," *Journal of the American Chemical Society* **124,** 4958–4959 (2002).

[23] M. R. Beversluis, A. Bouhelier, and L. Novotny, "Continuum generation from single gold nanostructures through near-field mediated intraband transitions," *Physical Review B* **68,** 115433 (2003).

[24] C. Anceau, S. Brasselet, J. Zyss, and P. Gadenne, "Local second-harmonic generation enhancement on gold nanostructures probed by two-photon microscopy," *Optics Letters* **28,** 713–715 (2003).

[25] H. Steffes, A. Schleunitz, U. Gernert, R. Chabicovsky, and E. Obermeier, "A novel optical gas sensor based on sputtered $In_xO_yN_z$ films with gold-nano-dots," *Microelectronic Engineering* **83,** 1197–1200 (2006).

[26] B. K. Canfield, H. Husu, J. Laukkanen, B. Bai, M. Kuittinen, J. Turunen, and M. Kauranen, "Local Field Asymmetry Drives Second-Harmonic Generation in Noncentrosymmetric Nanodimers," *Nano Letters* **7,** 1251–1255 (2007).

[27] B. K. Canfield, S. Kujala, H. Husu, M. Kauranen, B. Bai, J. Laukkanen, M. Kuittinen, Y. Svirko, and J. Turunen, "Local-field and multipolar effects in the second-harmonic response of arrays of metal nanoparticles," *Journal of Nonlinear Optical Physics & Materials* **16,** 317–328 (2007).

[28] H. Husu, B. K. Canfield, J. Laukkanen, B. Bai, M. Kuittinen, J. Turunen, and M. Kauranen, "Local-field effects in the nonlinear optical response of metamaterials," *Metamaterials* **2,** 155–168 (2008).

[29] H. Husu, B. K. Canfield, J. Laukkanen, B. Bai, M. Kuittinen, J. Turunen, and M. Kauranen, "Chiral coupling in gold nanodimers," *Applied Physics Letters* **93,** 183115 (2008).

[30] K. Jefimovs, J. Laukkanen, T. Vallius, T. Pilvi, M. Ritala, T. Meilahti, M. Kaipiainen, M. Bavdaz, M. Leskelä, and J. Turunen, "Free-standing inductive grid filter for infrared radiation rejection," *Microelectronic Engineering* **83,** 1339–1342 (2006).

[31] B. Bai, J. Laukkanen, A. Lehmuskero, X. Li, and J. Turunen, "Polarization-selective window-mirror effect in inductive gold grids," *Physical Review B* **81,** 235423 (2010).

[32] B. Bai, J. Laukkanen, A. Lehmuskero, and J. Turunen, "Simultaneously enhanced transmission and artificial optical activity in gold film perforated with chiral hole array," *Physical Review B* **81,** 115424 (2010).

[33] B. Bai, X. Meng, J. Laukkanen, T. Sfez, L. Yu, W. Nakagawa, H. P. Herzig, L. Li, and J. Turunen, "Asymmetrical excitation of surface plasmon polaritons on blazed gratings at normal incidence," *Physical Review B* **80,** 035407 (2009).

[34] J. Pietarinen, S. Siitonen, N. Tossavainen, J. Laukkanen, and M. Kuittinen, "Fabrication of Ni-shims using UV-moulding as an intermediate step," *Microelectronic Engineering* **83,** 492–498 (2006).

[35] J. Viheriälä, T. Niemi, J. Laukkanen, M. Karjalainen, and M. Pessa, "Large-area nanoperforated SiN membranes for optical and mechanical filtering," *Microelectronic Engineering* **87,** 1620–1622 (2010).

[36] L. Sainiemi, J. Viheriälä, T. Sikanen, J. Laukkanen, and T. Niemi, "Nanoperforated silicon membranes fabricated by UV-nanoimprint lithography, deep reactive ion etching and atomic layer deposition," *Journal of Micromechanics and Microengineering* **20,** 077001 (2010).

[37] L. Mandel and E. Wolf, *Optical coherence and quantum optics* (Cambridge University Press, Cambridge, 1995).

[38] S. A. Maier, *Plasmonics: Fundamentals and Applications* (Springer, New York, 2007).

[39] A. Ishikawa, T. Tanaka, and S. Kawata, "Negative Magnetic Permeability in the Visible Light Region," *Physical Review Letters* **95,** 237401 (2005).

[40] H. Du, J. Gong, C. Sun, R. Huang, and L. Wen, "Carrier Density and Plasma Frequency of Aluminum Nanofilms," *Journal of Material Science & Technology* **19,** 365–367 (2003).

[41] M. I. Markovic and A. D. Rakic, "Determination of the reflection coefficients of laser light of wavelengths $\lambda\epsilon(0.22\ \mu\text{m}, 200\ \mu\text{m})$ from the surface of aluminum using the Lorentz-Drude model," *Applied Optics* **29,** 3479–3483 (1990).

[42] A. V. Zayats and I. I. Smolyaninov, "Near-field photonics: surface plasmon polaritons and localized surface plasmons," *Journal of Optics A: Pure and Applied Optics* **5,** S16–S50 (2003).

[43] J. R. Sambles, G. W. Bradbery, and F. Yang, "optical excitation of surface plasmons: an introduction," *Contemporary Physics* **32,** 173–183 (1991).

[44] R. W. Boyd, *Nonlinear Optics*, Second ed. (Academic Press, San Diego, 2003).

[45] P. A. Franken, A. E. Hill, C. W. Peters, and G. Weinreich, "Generation of Optical Harmonics," *Physical Review Letters* **7,** 118–119 (1961).

[46] A. Lehmuskero, M. Kuittinen, and P. Vahimaa, "Refractive index and extinction coefficient dependence of thin Al and Ir films on deposition technique and thickness," *Optics Express* **15,** 10744–10752 (2007).

[47] *CRC Handbook of Chemistry and Physics*, 64th ed. (CRC Press, Boca Ratow, 1984).

[48] V. Kettunen, M. Kuittinen, J. Turunen, and P. Vahimaa, "Spectral filtering with finitely conducting inductive grids," *Journal of the Optical Society of America A* **15,** 2783–2785 (1998).

[49] C. Rockstuhl, M. G. Salt, and H. P. Herzig, "Application of the boundary-element method to the interaction of light with single and coupled metallic nanoparticles," *Journal of the Optical Society of America A* **20,** 1969–1973 (2003).

[50] W.-H. Yang, G. C. Schatz, and R. P. Van Duyne, "Discrete dipole approximation for calculating extinction and Raman intensities for small particles with arbitrary shapes.," *Journal of Chemical Physics* **103,** 869 (1995).

[51] K. Shlager and J. Schneider, "A selective survey of the finite-difference time-domain literature," *Antennas and Propagation Magazine, IEEE* **37,** 39–57 (1995).

[52] S. A. Maier, P. G. Kik, and H. A. Atwater, "Optical pulse propagation in metal nanoparticle chain waveguides," *Physical Review B* **67,** 205402 (2003).

[53] E. Noponen and J. Turunen, "Eigenmode method for electromagnetic synthesis of diffractive elements with three-dimensional profiles," *Journal of the Optical Society of America A* **11,** 2494–2502 (1994).

[54] L. Li, "Use of Fourier series in the analysis of discontinuous periodic structures," *Journal of the Optical Society of America A* **13,** 1870–1876 (1996).

[55] L. Li, "New formulation of the Fourier modal method for crossed surface-relief gratings," *Journal of the Optical Society of America A* **14,** 2758–2767 (1997).

[56] B. Bai and L. Li, "Group-theoretic approach to enhancing the Fourier modal method for crossed gratings with C_4 symmetry," *Journal of Optics A: Pure and Applied Optics* **7,** 783 (2005).

[57] B. Bai and L. Li, "Reduction of computation time for crossed-grating problems: a group-theoretic approach," *Journal of the Optical Society of America A* **21,** 1886–1894 (2004).

[58] M. A. McCord and M. J. Rooks, "Electron Beam Lithography," Chap 2 in *Handbook of Microlithography, Micromachining, and Microfabrication*, Vol. 1: Microlithography, P. Rai-Choudhury, ed. (SPIE Optical Engineering Press, Washington, 1997).

[59] H. P. Herzig, E.-B. Kley, M. Clumme, and L. C. Wittig, "Micro-optics," Chap 3 in *MOEMS : micro-opto-electro-mechanical systems*, M. E. Motamedi, ed. (SPIE Press, Bellingham, 2005).

[60] A. Hohenau, H. Ditlbacher, B. Lamprecht, J. R. Krenn, A. Leitner, and F. R. Aussenegg, "Electron beam lithography, a helpful tool for nanooptics," *Microelectronic Engineering* **83,** 1464–1467 (2006).

[61] H. J. Levinson and W. H. Arnold, "Electron Beam Lithography," Chap 1 in *Handbook of Microlithography, Micromachining, and Microfabrication*, Vol. 1: Microlithography, P. Rai-Choudhury, ed. (SPIE Optical Engineering Press, Washington, 1997).

[62] M. J. Madou, *Fundamentals of Microfabrication: The Science of Miniturization*, Second ed. (CRC Press LLC, Boca Raton, 2002).

[63] A. Grigorescu, M. van der Krogt, C. Hagen, and P. Kruit, "10nm lines and spaces written in HSQ, using electron beam lithography," *Microelectronic Engineering* **84,** 822–824 (2007).

[64] S. Choi, M. Yan, L. Wang, and I. Adesida, "Ultra-dense hydrogen silsesquioxane (HSQ) structures on thin silicon nitride membranes," *Microelectronic Engineering* **86,** 521–523 (2009).

[65] T. R. Groves, D. Pickard, B. Rafferty, N. Crosland, D. Adam, and G. Schubert, "Maskless electron beam lithography: prospects, progress, and challenges," *Microelectronic Engineering* **61–62,** 285–293 (2002).

[66] S. Babin, M. Gaevski, D. Joy, M. Machin, and A. Martynov, "Technique to automatically measure electron-beam diameter and astigmatism: BEAMETR," *Journal of Vacuum Science & Technology B* **24,** 2956–2959 (2006).

[67] V. Sidorkin, A. van Run, A. van Langen-Suurling, A. Grigorescu, and E. van der Drift, "Towards 2-10nm electron-beam lithography: A quantitative approach," *Microelectronic Engineering* **85,** 805–809 (2008).

[68] J. S. Greeneich, "Electron-beam processes," Chap 2 in *Electron-Beam Technology in Microelectronic Fabrication*, G. R. Brewer, ed. (Academic Press, New York, 1980).

[69] J. Greeneich and T. Van Duzer, "An exposure model for electron-sensitive resists," *IEEE Transactions on Electron Devices* **21,** 286–299 (1974).

[70] T. H. P. Chang, "Proximity effect in electron-beam lithography," *Journal of Vacuum Science and Technology* **12,** 1271–1275 (1975).

[71] G. Owen, "Proximity effect correction in electron-beam lithography," *Optical Engineering* **32,** 2446–2451 (1993).

[72] S.-Y. Lee and K. Anbumony, "Analysis of three-dimensional proximity effect in electron-beam lithography," *Microelectronic Engineering* **83,** 336–344 (2006).

[73] W. M. Moreau, *Semiconductor Lithography: Principles, Practices, and Materials* (Plenum Press, New York, 1988).

[74] B. Niemann, T. Wilhein, T. Schliebe, R. Plontke, O. Fortagne, I. Stolberg, and M. Zierbock, "A special method to create gratings of variable line density by low voltage electron beam lithography," *Microelectronic Engineering* **30,** 49–52 (1996).

[75] E.-B. Kley, "Continuous profile writing by electron and optical lithography," *Microelectronic Engineering* **34,** 261–298 (1997).

[76] A. Nottola, A. Gerardino, M. Gentili, E. D. Fabrizio, S. Cabrini, P. Melpignano, and G. Rotaris, "Fabrication of semi-continuous profile Diffractive Optical Elements for beam shaping by Electron Beam Lithography," *Microelectronic Engineering* **53,** 325–328 (2000).

[77] W. Henschel, Y. M. Georgiev, and H. Kurz, "Study of a high contrast process for hydrogen silsesquioxane as a negative tone electron beam resist," *Journal of Vacuum Science & Technology B* **21,** 2018–2025 (2003).

[78] I. Haller, M. Hatzakis, and R. Srinivasan, "High-resolution Positive Resists for Electron-beam Exposure," *IBM Journal of Research and Development* **12,** 251–256 (1968).

[79] E. A. Dobisz, S. L. Brandow, R. Bass, and J. Mitterender, "Effects of molecular properties on nanolithography in polymethyl methacrylate," *Journal of Vacuum Science & Technology B* **18,** 107–111 (2000).

[80] S. Yasin, D. G. Hasko, and H. Ahmed, "Fabrication of <5 nm width lines in poly(methylmethacrylate) resist using a water:isopropyl alcohol developer and ultrasonically-assisted development," *Applied Physics Letters* **78,** 2760–2762 (2001).

[81] D. Küpper, D. Küpper, T. Wahlbrink, J. Bolten, M. C. Lemme, Y. M. Georgiev, and H. Kurz, "Megasonic-assisted development of nanostructures," *Journal of Vacuum Science & Technology B* **24,** 1827–1832 (2006).

[82] H. Namatsu, Y. Takahashi, K. Yamazaki, T. Yamaguchi, M. Nagase, and K. Kurihara, "Three-dimensional siloxane resist for the formation of nanopatterns with minimum linewidth fluctuations," *Journal of Vacuum Science & Technology B* **16,** 69–76 (1998).

[83] G. M. Schmid, L. E. Carpenter, II, and J. A. Liddle, "Non-aqueous development of silsesquioxane electron beam resist," *Journal of Vacuum Science & Technology B* **22,** 3497–3502 (2004).

[84] J. K. W. Yang and K. K. Berggren, "Using high-contrast salty development of hydrogen silsesquioxane for sub-10-nm half-pitch lithography," *Journal of Vacuum Science & Technology B* **25,** 2025–2029 (2007).

[85] A. E. Grigorescu, M. C. van der Krogt, C. W. Hagen, and P. Kruit, "Influence of the development process on ultimate resolution electron beam lithography, using ultrathin hydrogen silsesquioxane resist layers," *Journal of Vacuum Science & Technology B* **25,** 1998–2003 (2007).

[86] I.-B. Baek, J.-H. Yang, W.-J. Cho, C.-G. Ahn, K. Im, and S. Lee, "Electron beam lithography patterning of sub-10 nm line using hydrogen silsesquioxane for nanoscale device applications," *Journal of Vacuum Science & Technology B* **23,** 3120–3123 (2005).

[87] A. E. Grigorescu and C. W. Hagen, "Resists for sub-20-nm electron beam lithography with a focus on HSQ: state of the art," *Nanotechnology* **20,** 292001 (2009).

[88] F. C. M. J. M. van Delft, "Delay-time and aging effects on contrast and sensitivity of hydrogen silsesquioxane," *Journal of Vacuum Science & Technology B* **20,** 2932–2936 (2002).

[89] Y. Chen, H. Yang, and Z. Cui, "Effects of developing conditions on the contrast and sensitivity of hydrogen silsesquioxane," *Microelectronic Engineering* **83,** 1119–1123 (2006).

[90] F. Gaucher, A. Pautrat, S. Autier-Laurent, C. David, L. Calvet, P. Lecoeur, and A.-M. Haghiri-Gosnet, "Fabrication of metallic oxide nanowires," *Microelectronic Engineering* **86,** 820–823 (2009).

[91] W. Chao, J. Kim, S. Rekawa, P. Fischer, and E. Anderson, "Hydrogen silsesquioxane double patterning process for 12 nm resolution x-ray zone plates," *Journal of Vacuum Science & Technology B* **27,** 2606–2611 (2009).

[92] C. Vieu, F. Carcenac, A. Ppin, Y. Chen, M. Mejias, A. Lebib, L. Manin-Ferlazzo, L. Couraud, and H. Launois, "Electron beam lithography: resolution limits and applications," *Applied Surface Science* **164,** 111–117 (2000).

[93] F. Hua, J. Shi, Y. Lvov, and T. Cui, "Patterning of Layer-by-Layer Self-Assembled Multiple Types of Nanoparticle Thin Films by Lithographic Technique," *Nano Letters* **2,** 1219–1222 (2002).

[94] P. Carlberg, M. Graczyk, E. L. Sarwe, I. Maximov, M. Beck, and L. Montelius, "Lift-off process for nanoimprint lithography," *Microelectronic Engineering* **67–68,** 203–207 (2003).

[95] J. Henzie, M. H. Lee, and T. W. Odom, "Multiscale patterning of plasmonic metamaterials," *Nature Nanotechnology* **2,** 549–554 (2007).

[96] Y. Chen, K. Peng, and Z. Cui, "A lift-off process for high resolution patterns using PMMA/LOR resist stack," *Microelectronic Engineering* **73–74,** 278–281 (2004).

[97] R. Asthana, A. Kumar, and N. B. Dahotre, *Materials Processing and Manufacturing Science* (Elsevier, Burlington, 2006).

[98] I. W. Rangelow, "Critical tasks in high aspect ratio silicon dry etching for microelectromechanical systems," *Journal of Vacuum Science & Technology A* **21,** 1550–1562 (2003).

[99] G. S. Oehrlein, “Reactive Ion Etching,” Chap 8 in *Handbook of Plasma Processing Technology: Fundamental, Etching, Deposition and Surface Interactions*, S. M. Rossnagel, J. J. Cuomo, and W. D. Westwood, eds. (Noyes Publications, New York, 1990).

[100] Z. Ren, P. J. Heard, J. M. Marshall, P. A. Thomas, and S. Yu, “Etching characteristics of $LiNbO_3$ in reactive ion etching and inductively coupled plasma,” *Journal of Applied Physics* **103,** 034109 (2008).

[101] S. Choi, M. Yan, I. Adesida, K. H. Hsu, and N. X. Fang, “Ultradense gold nanostructures fabricated using hydrogen silsesquioxane resist and applications for surface-enhanced Raman spectroscopy,” *Journal of Vacuum Science & Technology B* **27,** 2640–2643 (2009).

[102] A. Milenin, C. Jamois, R. Wehrspohn, and M. Reiche, “The SOI planar photonic crystal fabrication: patterning of Cr using Cl2/O2 plasma etching,” *Microelectronic Engineering* **77,** 139–143 (2005).

[103] T. Wahlbrink, T. Mollenhauer, Y. Georgiev, W. Henschel, J. Efavi, H. Gottlob, M. Lemme, H. Kurz, J. Niehusmann, and P. H. Bolivar, “Highly selective etch process for silicon-on-insulator nano-devices,” *Microelectronic Engineering* **78–79,** 212–217 (2005).

[104] M. A. Vyvoda, H. Lee, M. V. Malyshev, F. P. Klemens, M. Cerullo, V. M. Donnelly, D. B. Graves, A. Kornblit, and J. T. C. Lee, “Effects of plasma conditions on the shapes of features etched in Cl_2 and HBr plasmas. I. Bulk crystalline silicon etching,” *Journal of Vacuum Science & Technology A* **16,** 3247–3258 (1998).

[105] G. D. Miller, R. G. Batchko, W. M. Tulloch, D. R. Weise, M. M. Fejer, and R. L. Byer, “42%-efficient single-pass cw second-harmonic generation in periodically poled lithium niobate,” *Optics Letters* **22,** 1834–1836 (1997).

[106] T. Levola and P. Laakkonen, "Replicated slanted gratings with a high refractive index material for in and outcoupling of light," *Optics Express* **15,** 2067–2074 (2007).

[107] X. Meng and L. Li, "In situ endpoint detection of reactive ion-beam etching of dielectric gratings with an etch-stop layer using downstream mass spectrometry," *Applied Surface Science* **254,** 5421–5425 (2008).

[108] L. J. Martínez, I. Prieto, B. Alén, and P. A. Postigo, "Fabrication of high quality factor photonic crystal microcavities in InAsP/InP membranes combining reactive ion beam etching and reactive ion etching," *Journal of Vacuum Science & Technology B* **27,** 1801–1804 (2009).

[109] D. S. Hines and K. E. Williams, "Patterning of wave guides in $LiNbO_3$ using ion beam etching and reactive ion beam etching," *Journal of Vacuum Science & Technology A* **20,** 1072–1075 (2002).

[110] H. M. Shang and G. Cao, "Template-Based Synthesis of Nanorod or Nanowire Arrays," Chap A5 in *Springer Handbook of Nanotechnology*, 2nd ed., B. Bhushan, ed. (Springer Science+Business Media, Inc., Berlin, 2007).

[111] P. Niranatlumpong and H. Koiprasert, "Improved corrosion resistance of thermally sprayed coating via surface grinding and electroplating techniques," *Surface and Coatings Technology* **201,** 737–743 (2006).

[112] S. Gorelick, J. Vila-Comamala, V. Guzenko, R. Mokso, M. Stampanoni, and C. David, "Direct e-beam writing of high aspect ratio nanostructures in PMMA: A tool for diffractive X-ray optics fabrication," *Microelectronic Engineering* **87,** 1052–1056 (2010).

[113] W. Bacher, W. Menz, and J. Mohr, "The LIGA technique and its potential for microsystems-a survey," *Industrial Electronics, IEEE Transactions on* **42,** 431–441 (1995).

[114] M. Leskelä and M. Ritala, "Atomic layer deposition (ALD): from precursors to thin film structures," *Thin Solid Films* **409,** 138–146 (2002).

[115] M. Ritala and M. Leskelä, "Atomic layer deposition," Chap 2 in *Handbook of Thin Films*, H. S. Nalwa, ed. (Academic Press, Burlington, 2002).

[116] M. Knez, K. Nielsch, and L. Niinistö, "Synthesis and Surface Engineering of Complex Nanostructures by Atomic Layer Deposition," *Advanced Materials* **19,** 3425–3438 (2007).

[117] T. Alasaarela, A. Säynätjoki, T. Hakkarainen, and S. Honkanen, "Feature size reduction of silicon slot waveguides by partial filling using atomic layer deposition," *Optical Engineering* **48,** 080502 (2009).

[118] M. Born and E. Wolf, *Principles of optics : Electromagnetic theory of propagation, interference and diffraction of light*, 7th ed. (Cambridge University Press, Oxford, 1999).

[119] K. Li, M. I. Stockman, and D. J. Bergman, "Enhanced second harmonic generation in a self-similar chain of metal nanospheres," *Physical Review B* **72,** 153401 (2005).

[120] I. Romero, J. Aizpurua, G. W. Bryant, and F. J. G. D. Abajo, "Plasmons in nearly touching metallic nanoparticles: singular response in the limit of touching dimers," *Optics Express* **14,** 9988–9999 (2006).

[121] A. Lesuffleur, L. K. S. Kumar, and R. Gordon, "Enhanced second harmonic generation from nanoscale double-hole arrays in a gold film," *Applied Physics Letters* **88,** 261104 (2006).

[122] M. Kauranen, T. Verbiest, and A. Persoons, "Second-order nonlinear optical signatures of surface chirality," *Journal of Modern Optics* **45,** 403–423 (1998).

[123] T. W. Ebbesen, H. J. Lezec, H. F. Ghaemi, T. Thio, , and P. A. Wolff, “Extraordinary optical transmission through subwavelength hole arrays,” *Nature* **391,** 667–669 (1998).

[124] Q. Cao and P. Lalanne, “Negative Role of Surface Plasmons in the Transmission of Metallic Gratings with Very Narrow Slits,” *Physical Review Letters* **88,** 057403 (2002).

[125] P. Lalanne, J. C. Rodier, and J. P. Hugonin, “Surface plasmons of metallic surfaces perforated by nanohole arrays,” *Journal of Optics A: Pure and Applied Optics* **7,** 422 (2005).

[126] W. L. Barnes, W. A. Murray, J. Dintinger, E. Devaux, and T. W. Ebbesen, “Surface Plasmon Polaritons and Their Role in the Enhanced Transmission of Light through Periodic Arrays of Subwavelength Holes in a Metal Film,” *Physical Review Letters* **92,** 107401 (2004).

[127] C.-p. Huang, Q.-j. Wang, and Y.-y. Zhu, “Dual effect of surface plasmons in light transmission through perforated metal films,” *Physical Review B* **75,** 245421 (2007).

[128] C. Genet, M. P. van Exter, and J. P. Woerdman, “Fano-type interpretation of red shifts and red tails in hole array transmission spectra,” *Optics Communications* **225,** 331–336 (2003).

[129] M. Sarrazin, J.-P. Vigneron, and J.-M. Vigoureux, “Role of Wood anomalies in optical properties of thin metallic films with a bidimensional array of subwavelength holes,” *Physical Review B* **67,** 085415 (2003).

[130] P. B. Catrysse and S. Fan, “Near-complete transmission through subwavelength hole arrays in phonon-polaritonic thin films,” *Physical Review B* **75,** 075422 (2007).

[131] M. Kuwata-Gonokami, N. Saito, Y. Ino, M. Kauranen, K. Jefimovs, T. Vallius, J. Turunen, and Y. Svirko, “Giant Optical Activity in Quasi-Two-Dimensional Planar Nanostructures,” *Physical Review Letters* **95,** 227401 (2005).

[132] K. Konishi, T. Sugimoto, B. Bai, Y. Svirko, and M. Kuwata-Gonokami, "Effect of surface plasmon resonance on the optical activity of chiral metal nanogratings," *Optics Express* **15,** 9575–9583 (2007).

[133] A. Papakostas, A. Potts, D. M. Bagnall, S. L. Prosvirnin, H. J. Coles, and N. I. Zheludev, "Optical Manifestations of Planar Chirality," *Physical Review Letters* **90,** 107404 (2003).

[134] M. Decker, M. W. Klein, M. Wegener, and S. Linden, "Circular dichroism of planar chiral magnetic metamaterials," *Optics Letters* **32,** 856–858 (2007).

[135] V. A. Fedotov, A. S. Schwanecke, N. I. Zheludev, V. V. Khardikov, and S. L. Prosvirnin, "Asymmetric Transmission of Light and Enantiomerically Sensitive Plasmon Resonance in Planar Chiral Nanostructures," *Nano Letters* **7,** 1996 (2007).

[136] W. L. Barnes, A. Dereux, and T. W. Ebbesen, "Surface plasmon subwavelength optics," *Nature* **424,** 824–830 (2003).

[137] D. Egorov, B. S. Dennis, G. Blumberg, and M. I. Haftel, "Two-dimensional control of surface plasmons and directional beaming from arrays of subwavelength apertures," *Physical Review B* **70,** 033404 (2004).

[138] J.-Y. Laluet, E. Devaux, C. Genet, T. W. Ebbesen, J.-C. Weeber, and A. Dereux, "Optimization of surface plasmons launching from subwavelength hole arrays: modelling and experiments," *Optics Express* **15,** 3488–3495 (2007).

[139] B. H. Kleemann, J. Ruoff, and R. Arnold, "Area-coded effective medium structures, a new type of grating design," *Optics Letters* **30,** 1617–1619 (2005).

[140] H. Elfström, M. Kuittinen, T. Vallius, B. H. Kleemann, J. Ruoff, and R. Arnold, "Fabrication of blazed gratings by area-coded effective medium structures," *Optics Communications* **266,** 697–703 (2006).

[141] M. T. Gale, “Replication techniques for diffractive optical elements,” *Microelectronic Engineering* **34,** 321–339 (1997).

[142] L. J. Heyderman, H. Schift, C. David, J. Gobrecht, and T. Schweizer, “Flow behaviour of thin polymer films used for hot embossing lithography,” *Microelectronic Engineering* **54,** 229–245 (2000).

[143] N. Roos, H. Schulz, L. Bendfeldt, M. Fink, K. Pfeiffer, and H. C. Scheer, “First and second generation purely thermoset stamps for hot embossing,” *Microelectronic Engineering* **61–62,** 399–405 (2002).

[144] K.-H. Brenner, M. Kufner, S. Kufner, J. Moisel, A. Müller, S. Sinzinger, M. Testorf, J. Göttert, and J. Mohr, “Application of three-dimensional micro-optical components formed by lithography, electroforming, and plastic molding,” *Applied Optics* **32,** 6464–6469 (1993).

[145] Y. K. Shen and W. Y. Wu, “An Analysis Of The Three-dimensional Micro-injection Molding,” *International Communications in Heat and Mass Transfer* **29,** 423–431 (2002).

[146] S. Rudschuck, D. Hirsch, K. Zimmer, K. Otte, A. Braun, R. Mehnert, and F. Bigl, “Replication of 3D-micro- and nanostructures using different UV-curable polymers,” *Microelectronic Engineering* **53,** 557–560 (2000).

[147] C. Elsner, J. Dienelt, and D. Hirsch, “3D-microstructure replication processes using UV-curable acrylates,” *Microelectronic Engineering* **65,** 163–170 (2003).

[148] F. Nikolajeff, S. Jacobsson, S. Hård, Å. Billman, L. Lundbladh, and C. Lindell, “Replication of continuous-relief diffractive optical elements by conventional compact disc injection-molding techniques,” *Applied Optics* **36,** 4655–4659 (1997).

[149] J. Pietarinen, V. Kalima, T. T. Pakkanen, and M. Kuittinen, “Improvement of UV-moulding accuracy by heat and sol-

vent assisted process," *Microelectronic Engineering* **85,** 263–270 (2008).

[150] S. H. Ahn and L. J. Guo, "Large-Area Roll-to-Roll and Roll-to-Plate Nanoimprint Lithography: A Step toward High-Throughput Application of Continuous Nanoimprinting," *ACS Nano* **3,** 2304–2310 (2009).

[151] R. A. Pala, K. T. Shimizu, N. A. Melosh, and M. L. Brongersma, "A Nonvolatile Plasmonic Switch Employing Photochromic Molecules," *Nano Letters* **8,** 1506–1510 (2008).

Janne Laukkanen

Fabrication of metallic micro- and nanostructures for optical solutions

This dissertation is focused on the fabrication of metallic micro- and nanostructures. Patterning of the structures was done by electron beam lithography. Several fabrication methods of metal structures, including lift-off and dry etching, are discussed. Metallic structures are considered as final elements used in optical measurements and as mask or mould structures for post processing. Several applications for the fabricated structures are presented.

UNIVERSITY OF
EASTERN FINLAND

Publications of the University of Eastern Finland
Dissertations in Forestry and Natural Sciences

isbn 978-952-61-0177-4
issnl 1798-5668
issn 1798-5668